

See discussions, stats, and author profiles for this publication at: <https://www.researchgate.net/publication/51827187>

# A "Sliding Scale Rule" for Selectivity among NO, CO, and O<sub>2</sub> by Heme Protein Sensors

ARTICLE *in* BIOCHEMISTRY · NOVEMBER 2011

Impact Factor: 3.02 · DOI: 10.1021/bi2015629 · Source: PubMed

---

CITATIONS

30

READS

72

---

## 4 AUTHORS, INCLUDING:



[Ah-Lim Tsai](#)

University of Texas Health Science Center at ...

142 PUBLICATIONS 4,610 CITATIONS

[SEE PROFILE](#)



[Emil Martin](#)

University of Texas Medical School

65 PUBLICATIONS 2,631 CITATIONS

[SEE PROFILE](#)



[John S. Olson](#)

Rice University

246 PUBLICATIONS 12,307 CITATIONS

[SEE PROFILE](#)

# A “Sliding Scale Rule” for Selectivity among NO, CO, and O<sub>2</sub> by Heme Protein Sensors

1 Ah-Lim Tsai,<sup>\*,†</sup> Vladimir Berka,<sup>†</sup> Emil Martin,<sup>‡</sup> and John S. Olson<sup>§</sup>

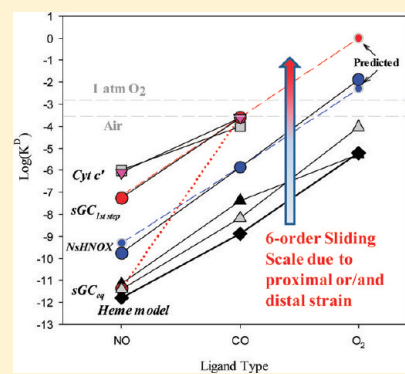
4 <sup>†</sup>Division of Hematology, Internal Medicine, University of Texas Medical School at Houston, Houston, Texas 77030, United States

5 <sup>‡</sup>Division of Cardiology, Internal Medicine, University of Texas Medical School at Houston, Houston, Texas 77030, United States

6 <sup>§</sup>Department of Biochemistry and Cell Biology, Rice University, Houston, Texas 77251-1892, United States

## 7 Supporting Information

8 **ABSTRACT:** Selectivity among NO, CO, and O<sub>2</sub> is crucial for the physiological  
 9 function of most heme proteins. Although there is a million-fold variation in  
 10 equilibrium dissociation constants ( $K_D$ ), the ratios for NO:CO:O<sub>2</sub> binding stay roughly  
 11 the same, 1: $\sim 10^3$ : $\sim 10^6$ , when the proximal ligand is a histidine and the distal site is  
 12 apolar. For these proteins, there is a “sliding scale rule” for plots of log( $K_D$ ) versus  
 13 ligand type that allows predictions of  $K_D$  values if one or two are missing. The predicted  
 14  $K_D$  for binding of O<sub>2</sub> to Ns H-NOX coincides with the value determined experimentally  
 15 at high pressures. Active site hydrogen bond donors break the rule and selectively  
 16 increase O<sub>2</sub> affinity with little effect on CO and NO binding. Strong field proximal  
 17 ligands such as thiolate, tyrosinate, and imidazolate exert a “leveling” effect on ligand  
 18 binding affinity. The reported picomolar  $K_D$  for binding of NO to sGC deviates even  
 19 more dramatically from the sliding scale rule, showing a NO:CO  $K_D$  ratio of 1: $\sim 10^8$ .  
 20 This deviation is explained by a complex, multistep process, in which an initial low-  
 21 affinity hexacoordinate NO complex with a measured  $K_D$  of  $\approx 54$  nM, matching that  
 22 predicted from the sliding scale rule, is formed initially and then is converted to a high-affinity pentacoordinate complex. This  
 23 multistep six-coordinate to five-coordinate mechanism appears to be common to all NO sensors that exclude O<sub>2</sub> binding to  
 24 capture a lower level of cellular NO and prevent its consumption by dioxygenation.



25 **T**he main biological functions of heme proteins are  
 26 transport, storage, sensing of key diatomic gaseous  
 27 molecules, and participation in redox reactions.<sup>1,2</sup> The high  
 28 reactivity of ferrous heme iron with dioxygen (O<sub>2</sub>) to produce  
 29 radicals precludes its presence as a free form in biological  
 30 systems to avoid adverse reactions that lead to oxidative stress.  
 31 Thus, in most cells, free heme is either quickly integrated into  
 32 proteins or rapidly degraded via the heme oxygenase pathway.  
 33 The protein not only sequesters the Fe-protoporphyrin ring,  
 34 but also provides specific axial ligands, steric constraints, and  
 35 electrostatic interactions that regulate exogenous ligand affinity,  
 36 heme iron redox potential, and the metal spin state.

37 Various protein structures have evolved to modulate the  
 38 intrinsic selectivity of pentacoordinate heme–His complexes  
 39 for the three major gaseous ligands, nitric oxide (NO), carbon  
 40 monoxide (CO), and O<sub>2</sub>, which differ by only one valence  
 41 electron between the CO and NO pair and the NO and O<sub>2</sub>  
 42 pair. The oxygen storage and delivery proteins, Mb and Hb,  
 43 respectively, use “electrostatic” discrimination to preferentially  
 44 stabilize bound O<sub>2</sub> via the donation of hydrogen bonds from  
 45 distal amino acids, normally histidine, tyrosine, or glutamine.<sup>3</sup>  
 46 In the NO-storing nitrophorins from the saliva of blood-  
 47 sucking insects, the heme is present in the oxidized form,  
 48 Fe(III)-protoporphyrin IX, which cannot bind either CO or O<sub>2</sub>,  
 49 but does permit a pH-dependent reversible uptake of NO and  
 50 displacement by histamine.<sup>4</sup> In the case of FixL, the oxygen

51 sensor found in nitrogen-fixing bacteria, the partial negative 52 charge on bound O<sub>2</sub> induces inward movement of a key Arg220 53 to form a favorable electrostatic interaction. This conformation 54 change triggers signaling and cannot be achieved by either NO 55 or CO binding because the resulting Fe(II)–ligand complexes 56 lack the strong polarizability of the Fe(II)<sup>δ(+)</sup>–O<sub>2</sub><sup>δ(-)</sup> complex.<sup>5</sup> 57 The CO-sensing protein CooA from phototropic bacteria 58 achieves CO selectivity using a reversible redox switch 59 mechanism. In contrast, binding of O<sub>2</sub> to CooA causes rapid 60 autoxidation to Fe(III) heme and superoxide formation, and 61 binding of NO leads to dissociation of the proximal ligand. 62 Neither of these latter events triggers signal transduction.<sup>6</sup> 63

The major target for NO signaling in mammals is sGC,<sup>7</sup> which binds NO, ruptures the proximal Fe–His bond, and triggers activation of cGMP formation. CO binding is weak and not capable of breaking the Fe–His coordination, whereas O<sub>2</sub> simply does not bind to reduced sGC.<sup>7</sup> Most remarkably, sGC manages to bind NO with an apparent  $K_D$  of  $\sim 4 \times 10^{-12}$  M (Table 1)<sup>8</sup> but excludes O<sub>2</sub>, a property that has not been explained mechanistically. We have addressed this property of sGC quantitatively by defining the general rules that govern ligand selectivity in heme proteins with a neutral proximal

Received: October 10, 2011

Revised: November 22, 2011

**Table 1.** Gaseous Ligand Binding Parameter Values for sGC,  $\alpha\beta$ I14SY sGC, Cytochrome  $c'$ , NS H-NOX, HemAT, Mb, H64V Mb, and Model Heme

sample	$K_D$ (M)	$k_{off}$ (s $^{-1}$ )	$k_{on}$ (M $^{-1}$ s $^{-1}$ )	refs and comments <sup>a</sup>
wild-type sGC				
NO	$4.2 \times 10^{-12}$ <sup>b</sup>	$5.4 \times 10^{-8}$ <sup>c</sup>	$6 \times 10^{-4}$ , 27 <sup>c</sup> -50 <sup>d</sup>	1.4 $\times 10^8$ <sup>c</sup> , 4.8 $\times 10^8$ 2.4 $\times 10^5$ , 1 $\times 10^{6d}$ 8, <sup>d</sup> 4 °C, <sup>d</sup> 9
CO	$2.6 \times 10^{-4}$	10.7	$4 \times 10^4$	9, 20, 21
O <sub>2</sub>	N/A	N/A	N/A	21
cytochrome $c'$				
NO	$1.2-9.1 \times 10^{-6}$	N/D	$4.4 \times 10^4$	24, 25, 27
CO	$2.8 \times 10^{-4}$	0.028	101	23, 26
O <sub>2</sub>	N/A	N/A	N/A	
$\alpha\beta$ I14SY sGC				
NO	$\leq 0.8 \times 10^{-6}$	≤10	$1.2 \times 10^7$	9
CO	$2.5 \times 10^{-4}$	0.8	$3 \times 10^3$	9
O <sub>2</sub>	N/A	N/A	N/A	9
NS H-NOX				
NO	$1.7 \times 10^{-10}$	0.05	$3 \times 10^8$	first 6C NO complex <sup>13</sup>
	$0.8 \times 10^{-6}$	1.9	$2.4 \times 10^6$	second 6C NO complex <sup>13</sup>
CO	$1.4 \times 10^{-6}$	3.6	$3 \times 10^6$	6C NO complex <sup>13</sup>
O <sub>2</sub>	$1.3 \times 10^{-2d}$	N/A	N/A	slow autoxidation <sup>13</sup>
HemAT				
NO	-	-	-	
CO	$1.6 \times 10^{-7}$	$7.0 \times 10^{-2}$	$4.3 \times 10^5$	28
O <sub>2</sub>	$9.1 \times 10^{-5}$	1800	$1.9 \times 10^7$	28
Y70FHemAT				
NO	-	-	-	
CO	$6.2 \times 10^{-8}$	$3.0 \times 10^{-2}$	$4.7 \times 10^5$	28
O <sub>2</sub>	$3.3 \times 10^{-4}$	19000	$5.3 \times 10^7$	28
Mb(II), whale				
NO	$4.5 \times 10^{-12}$	$1.0 \times 10^{-4}$	$2.2 \times 10^7$	18, 19
CO	$3.7 \times 10^{-8}$	$1.9 \times 10^{-2}$	$5.1 \times 10^5$	17, 18
O <sub>2</sub>	$0.9 \times 10^{-6}$	15	$1.7 \times 10^7$	17, 18
H64V Mb				
NO	$4.0 \times 10^{-12}$	$1.1 \times 10^{-3}$	$2.7 \times 10^8$	3, 18
CO	$6.8 \times 10^{-9}$	$4.8 \times 10^{-2}$	$7.0 \times 10^6$	3, 18
O <sub>2</sub>	$9.1 \times 10^{-5}$	10000	$1.1 \times 10^8$	3, 18
Fe(II)PP(1-MeIm)				
NO	$1.6 \times 10^{-12}$	$2.9 \times 10^{-4}$	$1.8 \times 10^8$	14, 16
CO	$1.3 \times 10^{-9}$	$2.3 \times 10^{-3}$	$1.8 \times 10^6$	14, 16
O <sub>2</sub>	$0.6 \times 10^{-5}$	310	$5.5 \times 10^7$	15

<sup>a</sup>Unless otherwise specified, the experimental temperature was 20–25 °C. <sup>b</sup>Calculated as  $k_{off}/k_{on}$  using values from refs 8 and 34. N/A, not applicable; N/D, not determined. <sup>c</sup>Calculated on the basis of  $k_{off}$  and  $k_{on}$  for 6c NO complex determined in this study at 24 °C. <sup>d</sup>Determined by an oxygen binding isotherm under high pressure in this study.

histidine–Fe(II) bond. The deviation of the NO binding properties of sGC from these rules requires a multistep binding mechanism, which explains how GC and heme-nitric oxide and oxygen binding (H-NOX) classes of heme-based protein sensors evolved such remarkably high selectivity for NO and against O<sub>2</sub>.

To verify the general rules and the multistep mechanism for the NO sensors, we re-examined the first step in binding of NO to sGC and re-evaluated the ligand binding properties of a panel of heme-based protein sensors, globins, and model heme. The almost linear relationship of log( $K_D$ ) for NO versus CO versus O<sub>2</sub> binding for most heme proteins suggests a “sliding scale rule”, which allows a prediction of the affinity of one ligand if  $K_D$  for the other ligand(s) is known. Deviations from this sliding scale rule are the result of stereochemical interactions with the surrounding protein elements that

enhance selectivity in favor of one of the gaseous ligands and sometimes against the others.

## METHODS

**Construction of the Expression Vector for His-Tagged Ns H-NOX.** The H-NOX of *Nostoc* sp. PCC 7120 (Ns H-NOX<sup>-189</sup>) gene sequence (GenBank accession number 17229770) was first optimized for *Escherichia coli* codon usage, replacing several rare codons with high-frequency synonymous codons to form a synthetic gene encoding Ns H-NOX. This optimized cDNA, together with six histidine codons inserted upstream of the stop codon (resulting in recombinant Ns H-NOX with a C-terminal His tag), was synthesized and cloned into the pBSK vector (Epoch LifeScience, Houston, TX). The Ns H-NOX cDNA was released by digestion with NdeI and XhoI and subcloned into pET43.1a (predigested with NdeI and XhoI). The integrity of



105 the resulting plasmid, designated pET43.1a-*Ns* H-NOX, was  
106 confirmed by restriction digestion and DNA sequencing.

107 **Expression and Purification of His-Tagged Recombi-**  
108 **nant *Ns* H-NOX, sGC, and Prostacyclin Synthase (PGIS).**

109 The *E. coli* C43(DE3)pLysS strain (Lucigen, Middleton, WI)  
110 was transformed with the pET43.1a-*Ns* H-NOX expression  
111 plasmid and grown overnight in Terrific Broth containing  
112 chloramphenicol (45  $\mu$ g/mL) and ampicillin (150  $\mu$ g/mL) at  
113 37 °C. The overnight culture (20 mL) was used to inoculate 1  
114 L of Terrific Broth containing ampicillin (150  $\mu$ g/mL) and  
115 incubated with shaking (200 rpm) at 37 °C until the  $A_{610}$   
116 reached 0.8. After the sample had been chilled to 20 °C, heme  
117 (2  $\mu$ M),  $\delta$ -aminolevulinic acid (0.2 mM), and isopropyl 1-thio-  
118  $\beta$ -D-galactopyranoside (IPTG, 1 mM) were added, and the  
119 culture was continued for 48 h at 18 °C with shaking at 200  
120 rpm. Cells were harvested by centrifugation and stored at -76  
121 °C.

122 Cells from 2 L of culture were resuspended in 125 mL of  
123 buffer A [100 mM potassium phosphate (pH 7.5), 100 mM  
124 NaCl, 10% glycerol, and 1 mM  $\beta$ -mercaptoethanol]. Egg  
125 lysozyme (150 mg in 5 mL of buffer A) was added and the  
126 suspension stirred at 4 °C for 1 h, then sonicated (10 min total,  
127 10 s intervals, 50% duty cycle), and then centrifuged at 100000*g*  
128 and 4 °C for 1 h. A 10 mL portion of TALON affinity resin was  
129 packed in a glass column (2.8 cm × 23 cm) and washed with 10  
130 volumes of deionized water and 10 volumes of buffer A. The  
131 cleared cell lysate containing recombinant *Ns* H-NOX was then  
132 added to the column, and the mixture was agitated gently for 2  
133 h at 4 °C on a rotating mixer. The liquid was then drained from  
134 the column and the resin washed twice by capping the ends and  
135 agitating with 10 volumes of buffer A for 15 min. Then, two  
136 similar wash steps were performed with 10 volumes of buffer A  
137 containing 5 mM imidazole. The His-tagged *Ns* H-NOX was  
138 eluted with 5 volumes of buffer A containing 250 mM  
139 imidazole and collected in 3 mL fractions. Fractions containing  
140 purified *Ns* H-NOX (based on the  $A_{418}/A_{280}$  ratio) were pooled  
141 and concentrated with a 30 kDa cutoff Centricon device. The  
142 concentrated *Ns* H-NOX was chromatographed on a 10-DG  
143 column pre-equilibrated with buffer A to remove imidazole and  
144 stored at -76 °C.

145 Soluble guanylyl cyclase (sGC), with a specific activity of  
146 13.5  $\mu$ mol of cGMP min<sup>-1</sup> (mg of sGC)<sup>-1</sup>, was prepared in 50  
147 mM triethanolamine (TEA) (pH 7.5), as previously described.<sup>9</sup>  
148 The purified enzyme is Sc ferrous ( $A_{431} = 110 \text{ mM}^{-1} \text{ cm}^{-1}$ ) and  
149 is inert to oxygen.

150 The recombinant human PGIS was prepared as described  
151 previously<sup>10</sup> with minor modifications in protein purification.<sup>11</sup>  
152 Briefly, the human PGIS cDNA was modified by replacing the  
153 hydrophobic amino-terminal segment of the first 17 residues  
154 with a seven-residue segment (MAKKTSS) favoring expression  
155 in *E. coli* and by adding a four-histidine tag at the carboxyl  
156 terminus. The modified cDNA was constructed in the pCW  
157 vector driven by *tac* promoter, and recombinant PGIS was  
158 purified to electrophoretic homogeneity with a nickel affinity  
159 column and CM-Sepharose column chromatography from  
160 which PGIS was eluted by 20 mM NaP<sub>i</sub> (pH 7.2) containing  
161 150 mM NaCl and 10% glycerol. Purified PGIS was stored at  
162 -70 °C. The protein concentration was spectrophotometrically  
163 determined using an  $\epsilon_{418}$  of 103  $\text{mM}^{-1} \text{ cm}^{-1}$ .

164 **Determination of Protein and Heme Content.** The  
165 total protein content was assayed with a Bio-Rad DC protein  
166 assay kit using bovine serum albumin as the standard. The  
167 heme content was determined by the pyridine hemochromate  
168 method using a difference absorbance coefficient (556–538  
169 nm) of 24.5  $\text{mM}^{-1} \text{ cm}^{-1}$ . All protein samples we used were  
170 checked to have a full complement of heme.

171 **Electrophoretic and Immunoblot Analyses.** Protein  
172 samples were prepared by mixing with electrophoresis sample  
173 buffer containing 4.3% SDS and 250 mM dithiothreitol and  
174 incubation for 2 h at 95 °C. Protein mixtures were separated by  
175 electrophoresis under denaturing conditions using 12%  
176 polyacrylamide gels, with the protein bands visualized by  
177 Coomassie blue staining.

178 **Anaerobic Sequential Stopped-Flow Method.** We  
179 determined  $k_{\text{off}}$ (NO) with an Applied Photophysics model  
180 SX-18MV stopped-flow instrument with a rapid-scan diode-  
181 array accessory. The sample handling unit was located inside an  
182 anaerobic chamber (model 110V, Coy Laboratory Products,  
183 Inc.) filled with 10% H<sub>2</sub> in N<sub>2</sub> and fitted with a palladium-based  
184 O<sub>2</sub> scrubber. A gas analyzer (model 10, Coy Laboratory  
185 Products, Inc.) tracked both the hydrogen level and the oxygen  
186 level to make sure that the latter is 0 ppm during the kinetic  
187 measurements. An sGC solution was prepared in an anaerobic  
188 glass titrator via five cycles of vacuum and argon replacement  
189 (30 s and 5 min, respectively). A 2 mM NO stock solution and  
190 a 1 mM CO stock solution in TEA buffer were prepared in  
191 glass tonometers by saturation first with pure nitrogen and then  
192 with NO (or CO) at 1 atm. The openings of the side arms of  
193 the tonometers were then sealed with a rubber septum, and  
194 they were transferred into the anaerobic chamber. An airtight  
195 disposable syringe with a needle was used to retrieve different  
196 amounts of the NO stock solution to prepare the NO solution  
197 used for kinetic measurements. Other details of the kinetic  
198 measurements are given in the main text and legend of Figure  
199 2.

200 **Determination of O<sub>2</sub> Binding Affinity for *Ns* H-NOX**  
201 and sGC under High Pressures. The custom-built pressure  
202 cell was equipped with antireflection-coated sapphire windows  
203 and had a path length of 1 mm as previously described.<sup>12</sup> In  
204 these experiments, 200  $\mu$ L of the ferrous form of *Ns* H-NOX  
205 (50  $\mu$ M) or sGC (10  $\mu$ M) was added to the pressure cell that  
206 was preflushed with pure oxygen and isolated from air by a  
207 screw metal joint and then engaged to the oxygen cylinder by a  
208 control valve. The oxygen pressure was varied from 0 to 135 psi  
209 (or 9.2 atm) in 20 psi increments. Optical spectra were  
210 recorded after each increment of oxygen pressure and  
211 equilibration for ~2 min as the pressurized cell was shaken.  
212 After 135 psi, the cell was open to the air pressure and the  
213 spectrum was recorded to check the reversibility.

214 **EPR Spectroscopy.** Liquid helium-temperature EPR spec-  
215 tra were recorded on a Bruker EMX spectrometer using a  
216 GFS600 transfer line and an ITC503 temperature controller.  
217 An Oxford ESP900 cryostat was used to accommodate the  
218 quartz sample tube in an ER 4116DM resonator.<sup>13</sup> The  
219 conditions for liquid helium (10 K) EPR measurements were as  
220 follows: frequency, 9.6 GHz; modulation amplitude, 10 G;  
221 modulation frequency, 100 kHz; and time constant, 0.33 s.

## ■ RESULTS

222 **Linear Logarithm Plots of  $K_D$ (NO),  $K_D$ (CO), and  $K_D$ (O<sub>2</sub>)**  
223 for Heme Proteins with a Neutral Proximal Histidine.

224 Logarithmic plots of equilibrium dissociation constants ( $K_D$ ),  
225 association rate constants ( $k_{\text{on}}$ ), and dissociation rate constants  
226 ( $k_{\text{off}}$ ) versus ligand type were constructed for a large series of  
227 ferrous heme proteins that contain a neutral proximal histidine  
228 ligand (see Figures 1 and 5–8 and Figures S1–S3 of the  
229 fi

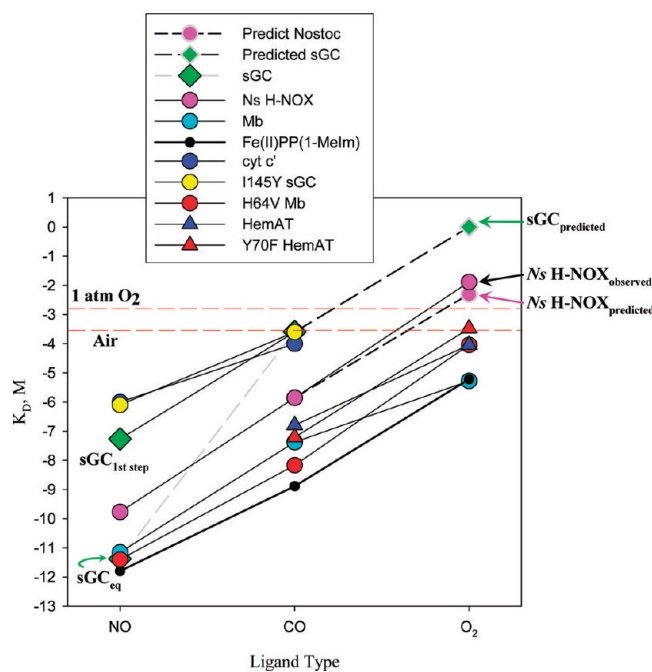


**Figure 1.** Sliding scale rule relationship of the dissociation equilibrium constants,  $K_D$ , of various heme sensors: Fe(II)PP(1-MeIm) (black circles and red line), Mb (cyan circles), H64V Mb (red circles), Ns H-NOX (pink circles), cyt c' (blue circles), I145Y sGC (yellow circles), HemAT (blue triangles), Y70F HemAT (red triangles), and sGC (green diamonds). Predicted  $K_D(O_2)$  values for sGC and Ns H-NOX were obtained by drawing parallel lines from the  $K_D(CO)$  to that of the model heme (black dashed lines and symbols with a gray edge). The ~4 order of magnitude difference in  $K_D(NO)$  between the 6c and final equilibrium 5c NO complexes formed in sGC is labeled and connected to  $K_D(CO)$  (solid vs dotted line).

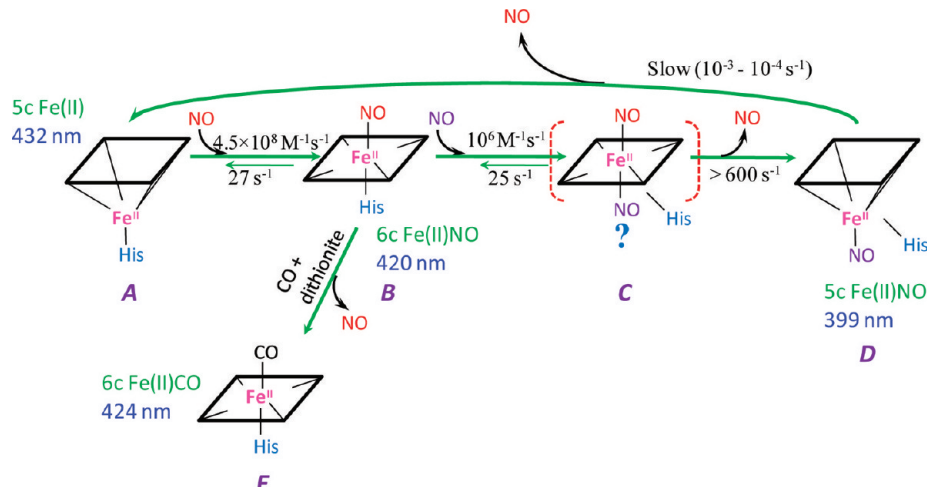
Supporting Information). In Figure 1, the  $K_D$  values for binding of NO, CO, and  $O_2$  to 5c Fe(II)PP(1-MeIm),<sup>14–16</sup> Mb,<sup>17–19</sup> sGC,<sup>8,9,20–22</sup> cytochrome c' (cyt c'),<sup>23–27</sup> and HemAT<sup>28</sup> were taken from the literature, and those for sGC containing the

I145Y mutation in the  $\beta$  subunit ( $\alpha\beta$ I145Y sGC)<sup>9</sup> and Ns H-NOX<sup>13</sup> were determined in our laboratory (Table 1). NO always shows the highest affinity (lowest  $K_D$ ) because of its radical nature and some back bonding; CO shows an intermediate affinity because of extensive back bonding, and  $O_2$  shows the lowest affinity because only a  $\sigma$  bond can be formed with the iron atom.<sup>29–31</sup> Although the absolute values of  $K_D$  vary more than 1 million-fold, i.e., six units along the  $y$ -axis in Figure 1, the  $K_D$  ratios of the CO and NO pair and the  $O_2$  and CO pair for each sample remain between  $10^3$  and  $10^4$ . This trend is shown most clearly for the Fe(II)PP(1-MeIm) model heme (thick line and small black circles, Figure 1) and leads to a “sliding” set of parallel lines for the NO to CO to  $O_2$  series for most of the proteins that have been examined.

Major exceptions to the linear log plots are observed when hydrogen bond donors are present in the active site, resulting in preferential stabilization of bound  $O_2$  and  $K_D(O_2)$  values smaller than those predicted by the sliding scale rule.<sup>3,18</sup> This effect is seen most clearly by the lower than expected  $K_D(O_2)$  for wild-type sperm whale myoglobin (swMb) with a distal histidine compared to the higher value for H64V Mb in which the active site is apolar (Figure 1, cyan vs red circles).<sup>32</sup> However, the  $K_D$  ratios for the CO and NO pair are relatively unchanged for these Mb variants. Similarly, in HemAT, the distal tyrosine stabilizes bound  $O_2$ , and when the tyrosine is replaced with phenylalanine, the apolar HemAT mutant shows a  $\log(K_D)$  plot perfectly parallel with those for H64V Mb and the model heme (Figure 1, blue vs red triangles).

Thus, for gas-binding heme proteins in the reduced, Fe(II) state, there appears to be a sliding scale rule, which prescribes parallel lines for plots of  $\log(K_D)$  for the NO to CO to  $O_2$  series. This relationship appears to apply to all 6c heme proteins and model hemes with a neutral proximal histidine ligand, and any decrease in the  $K_D(O_2)/K_D(CO)$  ratio is readily explained by preferential electrostatic stabilization of the polar Fe– $O_2$  complex. All other protein structural effects, including direct hindrance of the bound ligand, displacement of water from the active site, and proximal constraints of movements of iron–His species into and out of the plane of the heme, apply

### Scheme 1. Mechanism of the Multiple-Step Interaction between NO and sGC<sup>a</sup>



<sup>a</sup>Heme coordination structures and absorption maxima of the 6c CO complex (E) formed in excess CO and dithionite, starting 5c Fe(II)-bound sGC (A), the 6c NO complex (B), and the 5c NO complex at final equilibrium (D) are shown. The proposed transient 6c bis-NO complex (C, in brackets) is supported by the NO concentration dependence of the conversion from B to D and a recent <sup>15</sup>NO/<sup>14</sup>NO ligand binding EPR study (E. Martin et al., manuscript in revision). Numbers are rate constants at 24 °C determined in this study and one other recent sGC study.<sup>79</sup>

uniformly to the binding of all three ligands.<sup>33</sup> The only major exception to this rule is the remarkably large  $K_D(\text{CO})/K_D(\text{NO})$  ratio ( $\sim 10^7\text{--}10^8$ ) for equilibrium binding to sGC. This ratio is 4–5 orders of magnitude larger than that found for all the other heme proteins that have been examined (Figures 1, 7, and 8 and Figures S1–S3 of the Supporting Information). The binding of CO to sGC is very weak ( $K_D \approx 3 \times 10^{-4}$  M), and no binding of  $\text{O}_2$  to this protein has been detected. Thus, the predicted  $K_D$  for NO binding to form a ferrous 6c complex is  $\sim 3 \times 10^{-7}$  to  $10^{-8}$  M based on the sliding scale rule. In contrast, the reported  $K_D(\text{NO})$  value based on the ratio of published  $k_{\text{on}}$  and  $k_{\text{off}}$  values is  $10^{-12}$  M. This deviation from the sliding scale rule is a consequence of the multistep mechanism for binding of NO to sGC to form a 5c NO–heme complex, as first suggested by Traylor and Sharma (refs 8, 34, and 35).

### Measurements of $k_{\text{on}}$ and $k_{\text{off}}$ for the First NO Binding Step for sGC at Ambient Temperature.

The  $k_{\text{off}}$  reported in the literature for dissociation of NO from sGC refers to dissociation of the 5c NO–Fe(II) heme complex in its final equilibrium state (D in Scheme 1) and not to the labile 6c NO–Fe(II)-His complex transiently formed in the first step of NO binding<sup>8,34</sup> (C in Scheme 1). The  $k_{\text{off}}(\text{NO})$  values for the model heme, all the Mb variants, and the other heme proteins in Table 1 (and Figures 5–7 and Figures S1 and S2 of the Supporting Information) represent the rate of dissociation from bona fide 6c NO complexes. The  $k_{\text{off}}$  values for initial 6c NO–Fe(II)-His complexes can be reliably measured for cyt c,<sup>24,25</sup>  $\alpha\beta\text{I}145\text{Y}$  sGC,<sup>9</sup> and Ns H-NOX<sup>13</sup> (Table 1), because in these proteins the initial 6c NO complex is relatively stable and only slowly and partially converts to 5c NO–Fe(II) complexes at low NO:heme concentration ratios.

To resolve the dilemma of the abnormally large  $K_D(\text{CO})/K_D(\text{NO})$  of sGC, we determined both the on and off rate constants for the first step of binding of NO to sGC at 24 °C for comparison with the rate constants listed in Table 1, most of which were measured near room temperature. Because the  $k_{\text{on}}$  value is very large,<sup>8</sup> we had to conduct the kinetic measurements under second-order conditions, using an sGC:NO ratio of 1:1 and a final concentration at 0.5 μM each, to avoid missing most of the time course in the dead time of the stopped-flow apparatus. Measurements performed using either a rapid-scan diode array (Figure 2) or single-wavelength detection (Figure 2, inset) captured more than 60% of the total expected changes. The observed time courses were fitted to a second-order, irreversible mechanism (dashed line in Figure 2, inset) and yielded a  $k_{\text{on}}$  value of  $4.8 \times 10^8 \text{ M}^{-1} \text{ s}^{-1}$ , which is similar to the previously reported value of  $1.8 \times 10^8 \text{ M}^{-1} \text{ s}^{-1}$  measured 4 °C.<sup>8</sup>

To accurately measure the  $k_{\text{off}}$  for the initial 6c NO–sGC complex with a Soret peak at 420 nm, we maximized its formation in sequential stopped-flow mixing experiments. The 6c NO complex was generated by reacting 2 μM sGC with 2 μM NO in the first mixing step. The conversion of Fe(II)-bound sGC to the NO–Fe(II)-His complex (A → B in Scheme 1) was almost complete in the dead time of the stopped-flow apparatus (Figure 3A). This initial NO/sGC mixture was aged for 15–200 ms and then reacted with 1 mM CO and 25 mM dithionite to displace and consume dissociated NO, respectively (B → E in Scheme 1). After the second mixing step, an exponential increase in absorbance at 424 nm was observed, indicating formation of the CO–Fe(II)-His complex (E in Scheme 1) with a rate of  $\sim 27 \text{ s}^{-1}$  (Figure 3B). Increasing the aging time of the original 1:1 sGC/NO mixture to 200 ms led

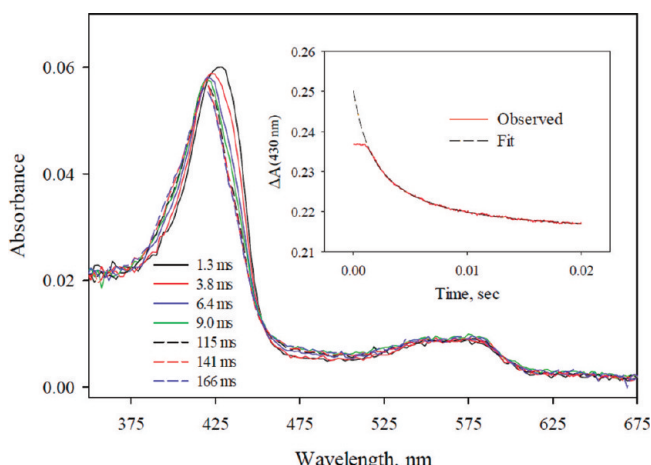


**Figure 2.** Time-dependent optical spectra of the reaction between 1 μM sGC and 1 μM NO (before mixing) at 23 °C recorded in the anaerobic rapid-scan stopped-flow apparatus. Spectra were recorded at 1.3–166 ms as indicated. Kinetic data of single-wavelength absorbance changes at 430 nm were also recorded (red trace in the inset) and fitted to a true second-order function (black dash in the inset) to obtain the rate constant.

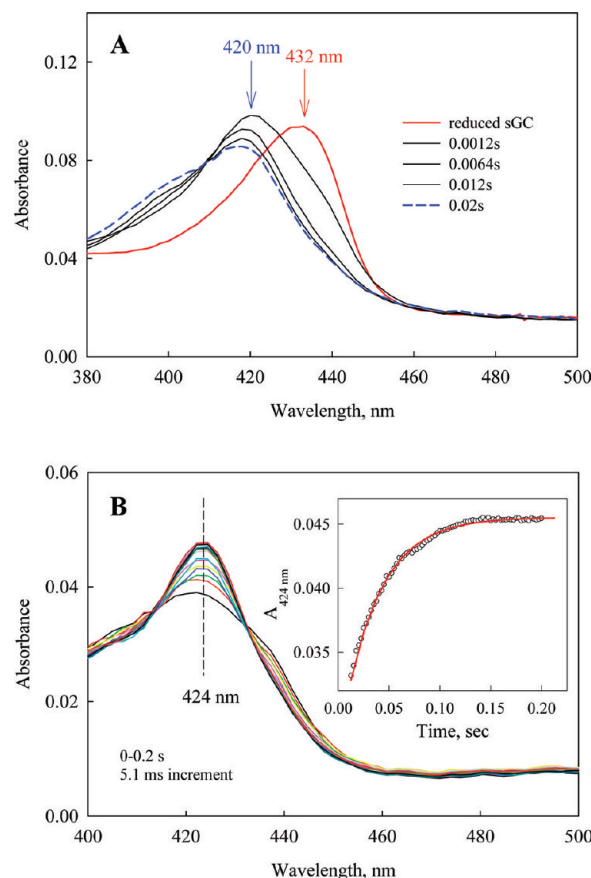


**Figure 3.** (A) Optical spectral changes during the reaction between sGC and a stoichiometric amount of NO. Rapid-scan stopped-flow data at 23 °C between 3.5 μM Fe(II)-bound sGC and stoichiometric NO were recorded. The peaks of Fe(II), the 6c NO complex, and the 5c NO complex are indicated. (B) Changes in optical spectra upon reaction between 2 μM sGC (premixed with stoichiometric NO) and 1 mM CO with 25 mM dithionite to determine the  $k_{\text{off}}(\text{NO})$  for the 6c-NO complex. Kinetic data at 424 nm changes with a 20 ms aging time are shown in the inset.

336 to little variation in the total absorbance change, the final peak  
 337 position, or the rate of NO displacement (Figure 3B, inset).  
 338 However, in each case, a small conversion to a Sc NO–Fe(II)  
 339 complex with a lower-intensity peak at 399 nm (a species  
 340 similar to D in Scheme 1 but with NO on the distal site of the  
 341 heme iron) occurs before the 6c NO–Fe(II)-His intermediate  
 342 is maximally formed. If the same sGC sample is reacted with an  
 343 excess of NO, a final equilibrium Sc NO–Fe(II) complex is  
 344 formed rapidly with a 399 nm absorbance band (D in Scheme  
 345 1) and little evidence of the 6c intermediates. Reaction of this  
 346 complex with 1 mM CO and 25 mM dithionite led to a  
 347 markedly smaller rate of NO dissociation, which is roughly  
 348 equal to that reported previously in the literature (i.e.,  $\sim 10^{-4}$   
 349  $s^{-1}$ )<sup>36</sup> (D → A in Scheme 1).

350 The  $k_{off}$ (NO) value of  $27 s^{-1}$  for the initial 6c NO complex  
 351 was used to calculate a  $K_D$ (NO) of  $5.4 \times 10^{-8} M$  for  
 352 dissociation of the initial NO–Fe(II)-His complex (Table 1  
 353 and Figure 1, green diamonds). When this value for the NO–  
 354 Fe(II)-His complex of sGC is used, the line connecting  
 355  $\log[K_D(\text{NO})]$  and  $\log[K_D(\text{CO})]$  becomes parallel with those  
 356 for all the other heme proteins studied and a 3–4 order of  
 357 magnitude intrinsic separation of the sGC  $K_D$  values between  
 358 the NO and CO pair and the CO and O<sub>2</sub> pair. Thus, the sliding  
 359 scale rule applies for 6c sGC complexes even though the  
 360 absolute values of the  $K_D$  values for each ligand are  $\sim 6$  orders  
 361 of magnitude larger than those for the model heme-imidazole  
 362 complex.

363 Linear extrapolation from the  $\log(K_D)$  values for NO and  
 364 CO binding predicts a  $K_D$  of  $\sim 1 M$  for binding of O<sub>2</sub> to sGC  
 365 (Figure 1, green diamonds with gray edges), which is 3 orders  
 366 of magnitude higher than the O<sub>2</sub> concentration in buffer  
 367 saturated with 1 atm of O<sub>2</sub> (Figure 1, horizontal red dashed  
 368 lines). Thus, when the 6c sGC complexes are examined, the  
 369 sliding scale rule predicts the exclusion of binding of oxygen by  
 370 sGC, and similar empirical predictions can be made for binding  
 371 of O<sub>2</sub> to I145Y sGC, cyt c', and Ns H-NOX, where the initial 6c  
 372 NO complexes are more easily examined.

373 **A Test of the Sliding Scale Rule: Binding of O<sub>2</sub> to Ns  
 374 H-NOX under High Pressures.** Ns H-NOX appears to be  
 375 unable to bind O<sub>2</sub> but does slowly autoxidize, indicating weak  
 376 interaction with O<sub>2</sub>.<sup>13</sup> Extrapolation from the observed  
 377  $K_D$ (CO) for Ns H-NOX by a line parallel to the data for the  
 378 other proteins in Figure 1 (pink circles with gray edges)  
 379 predicts that the  $K_D(O_2)$  for this sensor should be  $\sim 5$  mM. If  
 380 this prediction of the sliding scale rule is correct, then it should  
 381 be possible to detect binding of O<sub>2</sub> to Ns H-NOX spectrally  
 382 using only moderately high O<sub>2</sub> pressures. Spectral changes for  
 383 Fe(II)-bound Ns H-NOX were observed in a custom-built  
 384 pressure cell when  $P_{O_2}$  was increased from 0.2 to  $\sim 9$  atm (130  
 385 psi). The Soret band changed from a 430 nm band typical of 5c  
 386 Fe(II) heme to a broad band centered at 424 nm, which is not  
 387 the ferric form (Figure 4A). The absorbance difference  
 388 measured at 409–431 nm depends hyperbolically on O<sub>2</sub>  
 389 concentration and was consistent in four different experiments.  
 390 These data were analyzed with a simple one-step binding  
 391 function, and the fitted  $K_D$  of  $13 \times 10^{-3} M$  (Figure 4, inset) is  
 392 close to the value predicted by the sliding scale rule ( $\sim 5 \times 10^{-3}$   
 393 M). In contrast, when the same experiment was attempted with  
 394 sGC, no change in Soret absorbance was observed, even at 9.2  
 395 atm of pure O<sub>2</sub>, which is the highest limit before the sample  
 396 leaks from the pressure cell.

397 The lack of a characteristic visible spectrum typical of HbO<sub>2</sub>  
 398 complexes suggested that some oxidation might have occurred

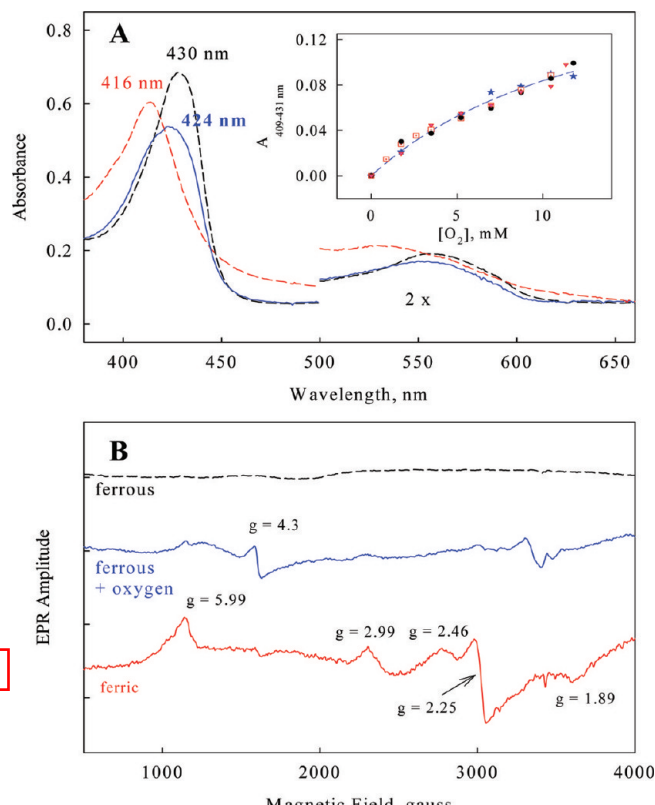


**Figure 4.** (A) Optical spectra of ferric (red dashed) and ferrous (black dashed) Ns H-NOX and ferrous Ns H-NOX under 135 psi of O<sub>2</sub> (blue) recorded in a high-pressure cell at 23 °C as described in Methods. (B) EPR spectra of ferric, ferrous, and oxygen-treated ferrous samples in panel A after they had been exposed to the air and transferred into an EPR tube. All samples were at 50 μM. EPR was recorded at 10 K, and the EPR condition is described in Methods.

in the Ns H-NOX samples, particularly at 9 atm of O<sub>2</sub>. EPR spectra of samples withdrawn from the pressure cell were recorded to quantify the amount of iron oxidation (Figure 4B). The oxygenated Ns H-NOX sample did exhibit small  $g = 6$  (high-spin) and  $g = 3$  and 2.25 (low-spin) signals for ferric heme and an increased amount of the denatured hemin–protein complex represented by the  $g = 4.3$  signal. However, the majority of the hemes were EPR-silent and present as either Sc Fe(II) or 6c Fe(II)O<sub>2</sub> complexes. Partial autoxidation and irreversible denaturation under treatment with high-pressure O<sub>2</sub> were confirmed by our failure to recover completely the original ferrous spectrum after the high O<sub>2</sub> pressure had been released (data not shown). Nonetheless, it is clear that most of the original unliganded Fe(II)-bound Ns H-NOX molecules do reversibly bind dioxygen with a  $K_D$  in the range of  $5–10 \times 10^{-3} M$ .

**Characteristic Dependence of Log( $k_{on}$ ) and Log( $k_{off}$ ) on Ligand Type.** Correlation plots for the logarithms of  $k_{on}$  and  $k_{off}$  show more complex shapes as a function of ligand type (Figure 5). The log( $k_{on}$ ) plots show vertical displacements of a “V-shaped” pattern, with the bimolecular rate constant for CO binding showing the smallest value, which is almost always 100–1000-fold smaller than  $k_{on}(\text{NO})$  and 10–100-fold smaller than  $k_{on}(O_2)$ . As described by Champion, Franzen, Harvey, and their co-workers,<sup>37–40</sup> the much smaller values of  $k_{on}(\text{CO})$  are due to both the requirement of in-plane movement of the heme iron to vacate the electron in the  $d_z^2$  orbital and the spin-

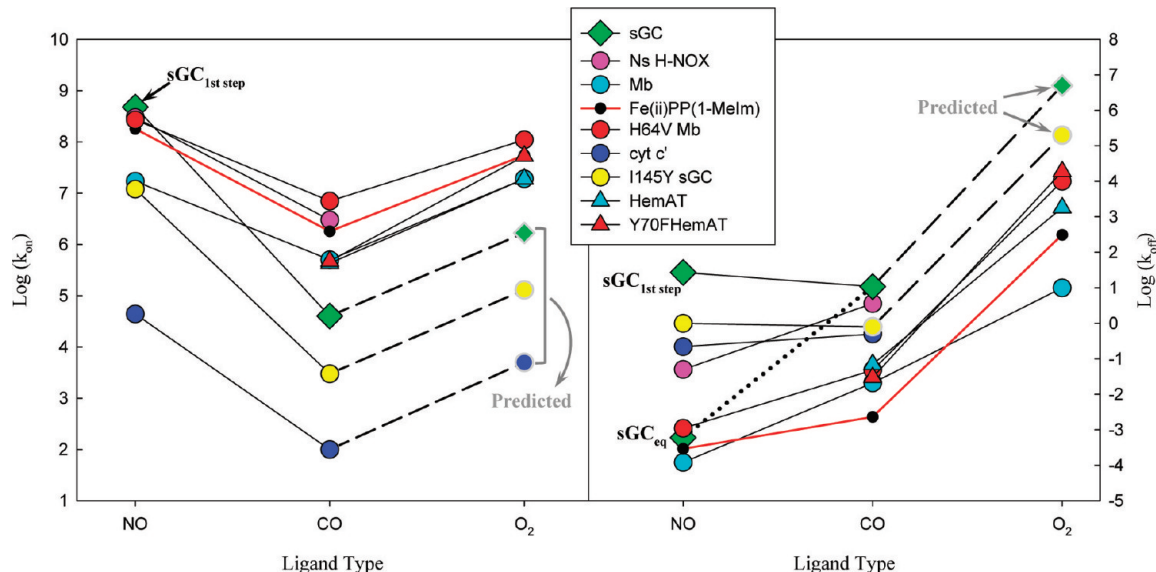


**Figure 5.** Relationship between  $\log(k_{\text{on}})$  [or  $\log(k_{\text{off}})$ ] values of various heme sensors and three ligand types. The predicted  $k_{\text{on}}$  (or  $k_{\text{off}}$ ) values are shown by dashed lines and symbols with gray edges. Other features match those in Figure 1.

forbidden nature of formation of an iron–carbonyl bond. As a result, the rate-limiting step for CO binding is formation of an internal bond with the iron atom. In contrast, bond formation can occur without a spin-state change in the iron when NO and O<sub>2</sub> are the ligands, because both contain unpaired electrons.<sup>37–40</sup> As a result, the rate of internal bond formation is very rapid for these ligands, and in the case of NO binding, the rate-limiting step for bimolecular association is migration of the ligand into the active site. In the case of O<sub>2</sub> binding,  $k_{\text{on}}$  can be limited by both ligand migration and bond formation, depending on the reactivity of the iron atom and steric restriction near the active site.<sup>41</sup> Thus, in most proteins,  $k_{\text{on}}(\text{NO}) \gg k_{\text{on}}(\text{CO}) < k_{\text{on}}(\text{O}_2)$  and a sliding V-shaped scale is seen.<sup>41</sup>

The pattern for  $\log(k_{\text{off}})$  is less clear and shows much greater variability in both the  $k_{\text{off}}(\text{CO})/k_{\text{off}}(\text{NO})$  and  $k_{\text{off}}(\text{O}_2)/k_{\text{off}}(\text{CO})$  ratios. However, in general,  $k_{\text{off}}(\text{NO}) \leq k_{\text{off}}(\text{CO}) \ll k_{\text{off}}(\text{O}_2)$ , so the pattern has characteristics of a “backward L”. In general, the rate constant for O<sub>2</sub> dissociation in heme proteins with an apolar active site is roughly 10<sup>6</sup>-fold greater than that for CO dissociation, and assuming this relationship holds for gas sensors, the predicted O<sub>2</sub> dissociation constant for sGC is estimated to be  $\sim 5 \times 10^6 \text{ s}^{-1}$  (Figure 5, right panel, dashed line and green diamonds with gray edges vs red line and black circles). The  $k_{\text{on}}(\text{O}_2)$  for sGC can then be estimated from this predicted  $k_{\text{off}}$  and the estimated  $K_D$  ( $\sim 1 \text{ M}$ ) from Figure 1. The resulting  $k_{\text{on}}$  value is  $\sim 2 \times 10^6 \text{ M}^{-1} \text{ s}^{-1}$  (Figure 5, left panel, green diamonds with gray edges), conforming well with the expected V shape for  $\log(k_{\text{on}})$  plots.

**Are the Sliding Scale Rules Applicable to All Globin Variants?** Over the past 20 years, the biochemical mechanisms for NO, CO, and O<sub>2</sub> binding have been examined systematically for large libraries of mammalian Mb and Hb variants.<sup>3,32,33</sup> As a test of the analysis in Figure 1, we constructed a graphical analysis for binding of NO, CO, and O<sub>2</sub> to 11 single Mb mutants, from a panel of 42 for which we have complete binding parameter values.<sup>42–44</sup> These 11 Mb mutants showed the largest changes in  $K_D$ ,  $k_{\text{on}}$ , or  $k_{\text{off}}$  compared to the wild-type (wt) Mb parameters. As shown in Figure 6A, the  $K_D(\text{NO})$  and  $K_D(\text{CO})$  values for these 11 mutants are highly

correlated in the ranges of  $10^{-10}$ – $10^{-12}$  and  $10^{-7}$ – $10^{-9} \text{ M}$ , respectively, showing parallel lines in the log plots.

In contrast, the  $\log[K_D(\text{O}_2)]$  values show significant deviations from the linear sliding scale rule. Marked decreases in  $K_D(\text{O}_2)$  are observed for those variants with an increased level of hydrogen bonding or favorable positive electrostatic fields, which preferentially stabilize bound O<sub>2</sub> (i.e., variants with His64 and Phe29). However, those Mb mutants with apolar distal pockets follow the expected linear sliding scale rule (Figure 6A, thick blue lines). The y-axis positions of the  $\log(K_D)$  values can be readily interpreted in terms of structural effects that regulate ligand affinity, all of which have been well-established for Mb<sup>3,32</sup> and are indicated by the arrows in Figure 6. Lower iron reactivity due to proximal constraints of in-plane movement, direct steric hindrance at the active site, and displacement of water from the distal pocket increase the  $K_D$  for the binding of all three gaseous ligands, whereas positive fields and hydrogen bond donors preferentially stabilize bound O<sub>2</sub>, causing a downward deflection of the last  $\log[K_D(\text{O}_2)]$  points in the plots (Figure 6A). Similar trends and explanations apply to all the other Mb variants that have been examined, and examples of these data are shown in Figures S1A and S2A of the Supporting Information for double and triple mutants.

Correlation plots for the bimolecular association ( $k_{\text{on}}$ ) and unimolecular dissociation ( $k_{\text{off}}$ ) rate constants for the same set of reduced Mb variants are shown in Figure 6B. The trends for  $\log(k_{\text{on}})$  are given in the left-hand panel, and the V shape is result of the differences in rate-limiting steps. Binding of NO to ferrous deoxyMb is limited only by the rate of entry into the protein active site; CO binding is limited by bond formation, and O<sub>2</sub> binding is partially limited by both processes. The bimolecular rate of ligand entry is governed by displacement of distal pocket water, diffusion into the distal pocket, and the size of the internal capture volume, whereas the rate of bond formation is governed by the reactivity of the iron atom (proximal effects) and steric hindrance at the open axial position. In the case of CO binding, the overall expression for  $k_{\text{on}}$  is  $k_{\text{bond}}K_{\text{entry}}$ , where  $K_{\text{entry}}$  is the equilibrium constant for noncovalent ligand binding in the active site, which also depends on the need to displace distal pocket water and the

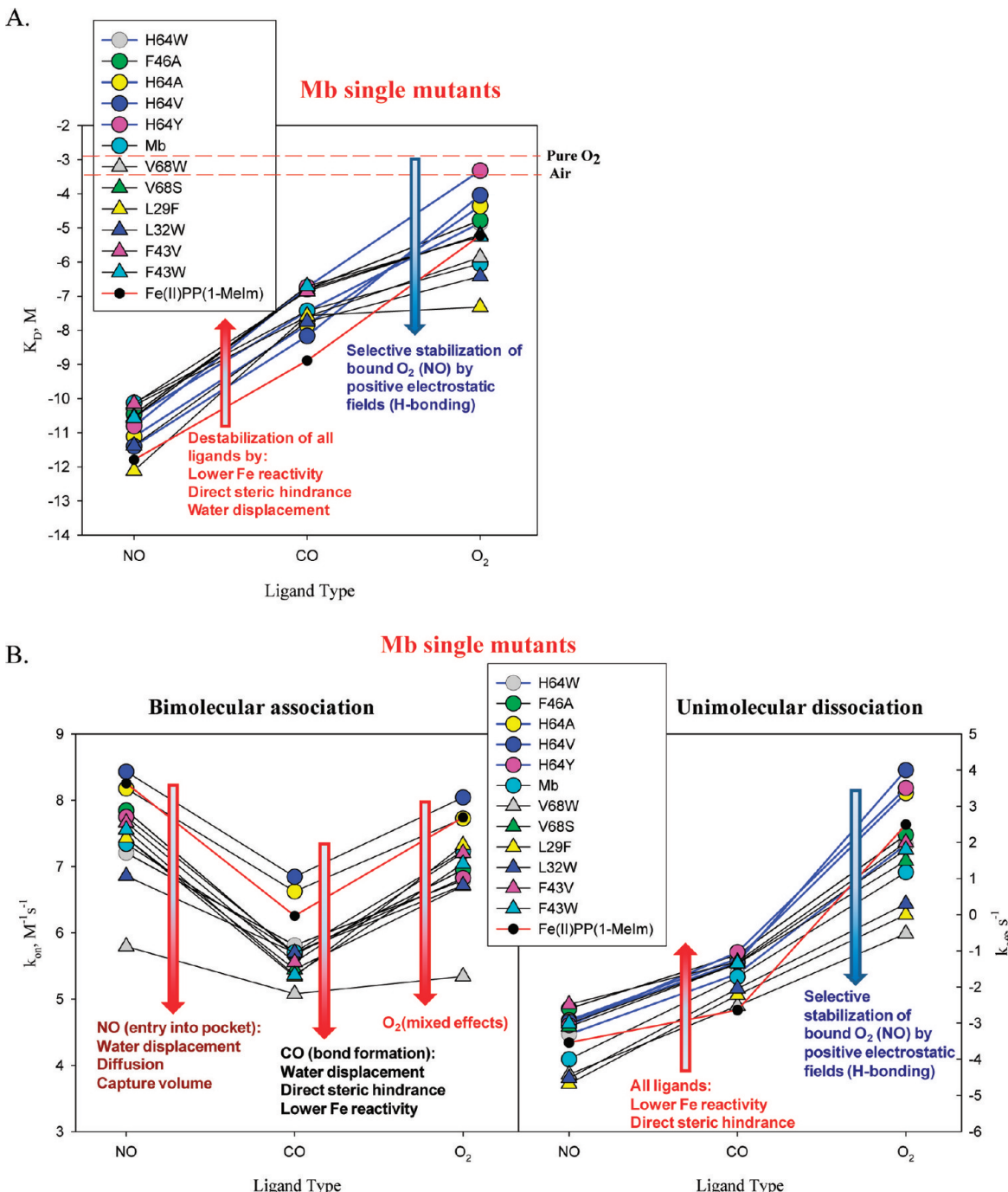


**Figure 6.** Categorical plot of either  $\log(K_D)$  (A) or  $\log(k_{on}/k_{off})$  (B) vs ligand type similar to Figure 1 for a panel of single mutants of Mb together with the model heme control (red line and black circles). Blue thick lines indicate the data of mutants with the key His64 changed to other residues. Binding parameter values are summarized in Table S1 of the Supporting Information.

active site volume.<sup>41</sup> Thus, when iron reactivity is lowered by proximal effects or direct hindrance, the depth of the V shape in the  $\log(k_{on})$  plot is greater because of the slight changes in  $k_{on}(NO)$  but large decreases in  $k_{on}(CO)$ . However, if the capture volume is decreased markedly as is the case for V68W Mb, all the rates are decreased dramatically and the V shape is much more shallow because slow ligand capture becomes limiting for all three ligands (Figure 6B, left panel, gray triangles).

The dominant variations seen in the  $\log(k_{off})$  plots are due to preferential electrostatic stabilization of bound  $O_2$ , causing

dramatic decreases in the absolute value of  $k_{off}(O_2)$  and the  $k_{off}(O_2)/k_{off}(CO)$  ratio (Figure 6B, right panel). In contrast, decreases in Fe(II) reactivity and direct steric hindrance of the bound ligand cause increases in  $k_{off}$  for all three ligands. There is some variability in  $k_{off}(NO)$  because the Fe(II)NO complex can be stabilized weakly by hydrogen bonding.<sup>3,45</sup> Again, similar correlation plots and interpretations can be made for libraries of double and triple mutants of sperm whale Mb, and the results all support the sliding scale rules (Figures S1 and S2 of the Supporting Information)

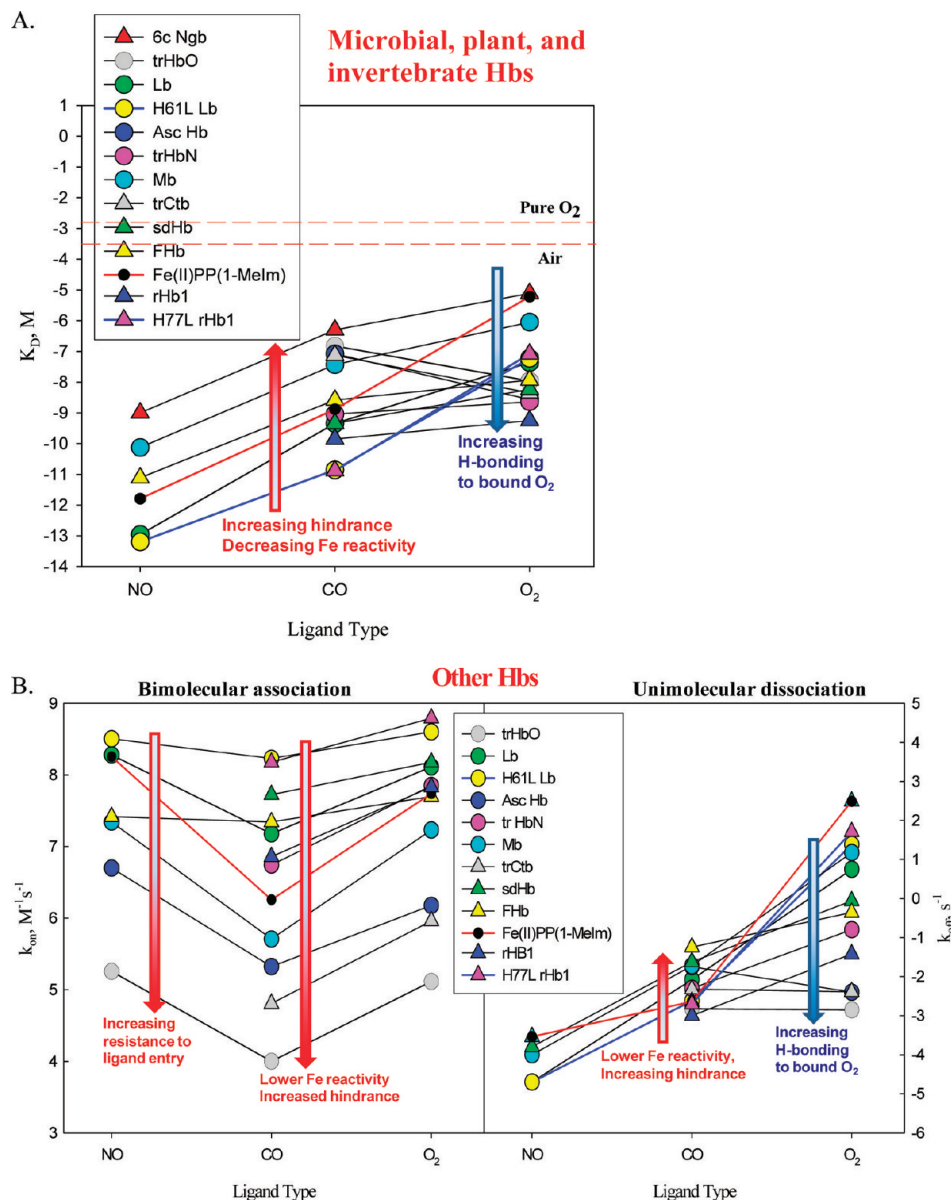


**Figure 7.** Categorical plot of either  $\log(K_D)$  (A) or  $\log(k_{on}/k_{off})$  (B) vs ligand type conducted for several globins: leghemoglobin (Lb, green circles) and its H61L mutant (yellow circles), rice hemoglobin type 1 (rHb1, blue triangles) and its H77L mutant (red triangles), Hb from *A. suum* (Asc Hb, blue circles), flavohemoglobin (FHb, yellow triangles) from bacteria and fungi, truncated Hb (trHb) from microorganisms, including trHbN (pink circles) and trHbO (gray circles) from *M. tuberculosis* and trCtb (gray triangles) and sdHb (green triangles) from *C. jejuni*, and even the 6c neuroglobin (Ngb, red triangles) together with Mb (cyan circles) and the model heme control (red line and black circles). Blue thick lines indicate the data of mutants with the key His64 changed to other residues. Binding parameter values are summarized in Table S2 of the Supporting Information.

As a more stringent test of the sliding scale analyses, we examined the ligand binding parameters for 11 different reduced globins from all kingdoms of life, including the plant hemoglobins, leghemoglobin (Lb)<sup>46</sup> and rice hemoglobin 1 (rHb1);<sup>47</sup> the invertebrate Hb from *Ascaris suum* (Asc Hb);<sup>19</sup> the flavohemoglobins (FHb) from bacteria and fungi; truncated Hbs (trHbs) from microorganisms, including trHbN and trHbO from *Mycobacterium tuberculosis* and trCtb, a single-domain hemoglobin from *Campylobacter jejuni*;<sup>48</sup> and human neuroglobin (Ngb)<sup>49</sup> (Figure 7 and Table S2 of the Supporting Information). There is a much greater range of absolute values for all the rate and equilibrium parameters, but the same rules and interpretations apply. For some of these globins, there are multiple hydrogen bonding interactions with bound O<sub>2</sub> leading

to dramatic decreases in  $K_D(O_2)$  and  $k_{off}(O_2)$  and  $K_D(O_2)/K_D(CO)$  and  $k_{off}(O_2)/k_{off}(CO)$  ratios of  $\leq 1.0$  (i.e., *Ascaris* Hb, trHbO, trHbN, rHb1, and trCtb). When the active site proton donors are replaced with apolar amino acids, the expected linear, V-shaped, and reverse L-shaped plots are observed for  $\log(K_D)$ ,  $\log(k_{on})$ , and  $\log(k_{off})$ , respectively (Figure 7, thick blue lines). These data, coupled with those for the Mb libraries and the heme proteins shown in Figure 1, argue strongly for the utility of the sliding scale analysis and its ability to predict ligand binding parameters if a set of  $K_D$ ,  $k_{off}$  and  $k_{on}$  parameters have been measured for CO binding and the polarity of the active site is known.

**Heme Proteins with a Thiolate Proximal Ligand Do Not Follow the Sliding Scale Rule.** There are limited and,

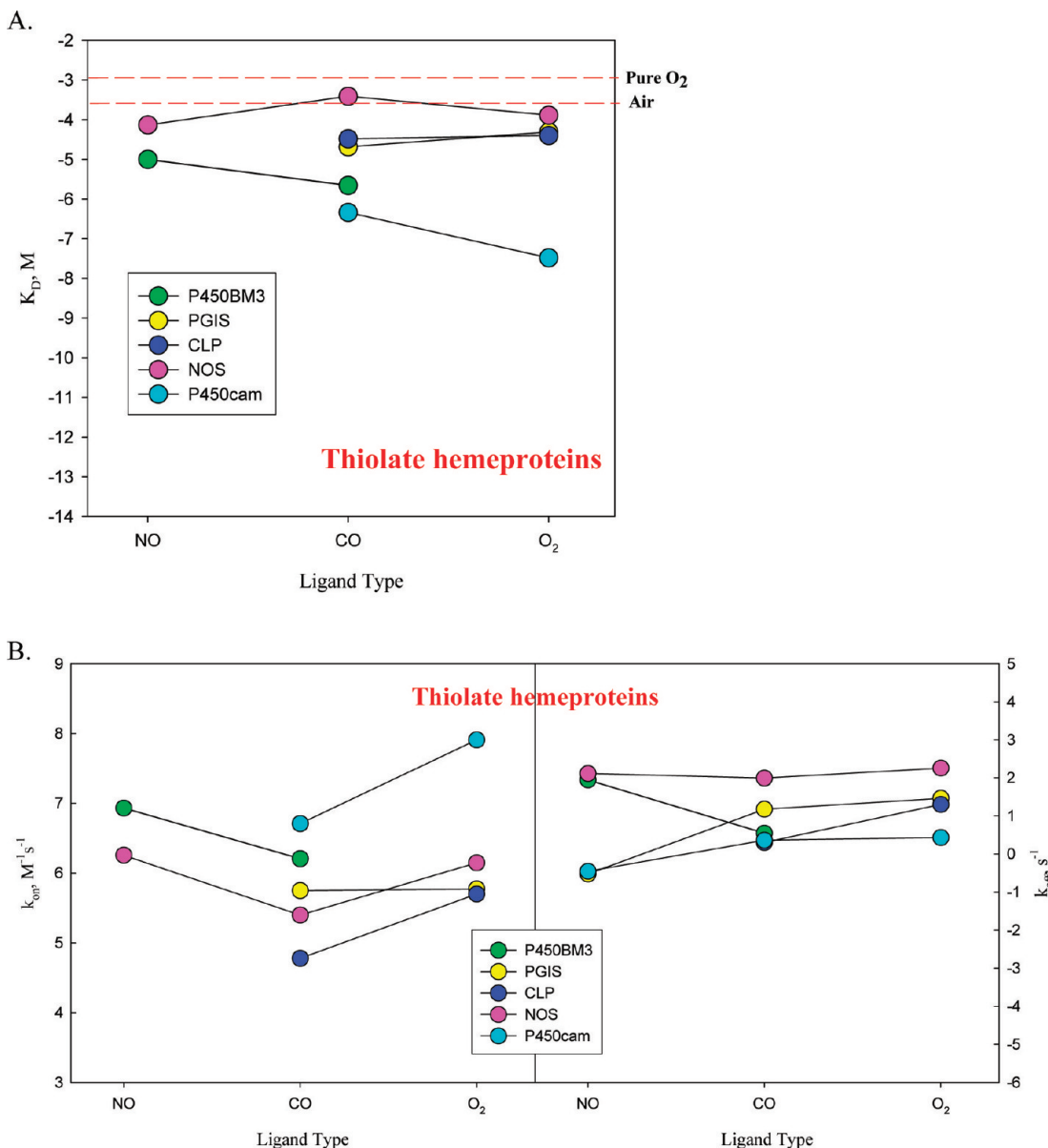


**Figure 8.** Categorical plot of either  $\log(K_D)$  (A) or  $\log(k_{on}/k_{off})$  (B) vs ligand type for several hemoproteins containing a thiolate proximal ligand, including cytochrome P450BM3 (green circles), prostacyclin synthase (PGIS, yellow circles), chloroperoxidase (CLP, blue circles), nitric oxide synthase (NOS, pink circles), and P450cam. Binding parameter values are summarized in Table S3 of the Supporting Information.

in most cases, incomplete kinetic data for binding of NO, CO, and O<sub>2</sub> to the reduced form of cytochrome P450 and P450-like proteins containing a proximal thiolate protein ligand. Nitric oxide synthase is the only one with a complete set of published binding parameters for all three ligands<sup>50,51</sup> (Table S3 of the Supporting Information).  $K_D$  and  $k_{on}$  values for only two gas ligands are available for Fe(II)-bound P450cam,<sup>52-54</sup> P450BM3,<sup>54,55</sup> chloroperoxidase (CLP),<sup>56,57</sup> and prostacyclin synthase (PGIS).<sup>58,59</sup> The  $k_{on}$ (NO) values for both P450cam and PGIS are  $\gg 10^8 \text{ M}^{-1} \text{ s}^{-1}$  (R. Van Eldik, personal communication, and our unpublished results, respectively) and cannot be determined by simple rapid-mixing methods; however, the  $k_{off}$ (NO) values could be determined for these two proteins. The ferric P450cam-NO complex was reduced with excess [Ru(EDTA)H<sub>2</sub>O]<sup>-</sup>, and  $k_{off}$ (NO) was determined to be  $0.35 \text{ s}^{-1}$ .<sup>52</sup> For PGIS, the ferrous protein was prepared by anaerobic titration with dithionite, and  $k_{off}$  was measured by

sequential mixing, stopped-flow protocols, as described for measuring  $k_{off}$ (NO) for the 6c NO complex of sGC (see Methods and Figure 3). A delay time of 0.5–1 s allowed us to maximize formation of the Fe(II)NO complex before the ligand was displaced by mixing with 1 mM CO and 40 mM dithionite. The kinetics of dissociation of CO from the ferrous PGIS-CO complex was determined to be  $0.3 \text{ s}^{-1}$  at 24 °C by mixing with buffer equilibrated with 1 atm of NO (Figure 8B, right).

Even with limited data, it is clear from Figure 8A and Table S3 of the Supporting Information that the  $\log(K_D)$  values for heme proteins with a proximal thiolate fail to follow the simple sliding scale rule observed for proteins with a proximal His (Figures 1 and 5–7). There is little variation in the  $K_D$  values for all three ligands, and  $K_D(O_2)$  is actually smaller than  $K_D(CO)$  for P450cam, even though there are no polar residues in the active site to stabilize bound dioxygen (Table S3 of the Supporting Information). Thiolate coordination seems to

abolish ligand binding selectivity. With the exception of that of PGIS, the  $k_{on}$  values seem to still follow the V shape sliding scale rule (Figure 8B, left panel), but the reversed L sliding scale relationship no longer holds for  $k_{off}$  values for P450-like heme proteins, for which there is a leveling effect causing the  $k_{off}$  values of all three ligands to be very similar (Figure 8B, right panel).

**Peroxidases Also Do Not Follow the Sliding Scale Rules.** We also analyzed data for five peroxidases, which have published binding parameters for at least two of the gas ligands (Table S4 of the Supporting Information). These enzymes include horseradish peroxidase (HRP),<sup>60,61</sup> lactoperoxidase (LPO),<sup>62,63</sup> eosinophil peroxidase (EPO),<sup>62</sup> cytochrome *c* peroxidase (CcP),<sup>64,65</sup> and myeloperoxidase (MPO).<sup>62,66</sup> In these proteins, the anionic imidazolate form of the proximal His side chain is coordinated to the iron atom due to the presence of ionized Asp and Glu side chains.<sup>67</sup> Plots of  $\log(K_D)$  versus ligand type for these enzymes show little variation and look similar to those for the P450-like heme proteins with a thiolate axial ligand (Figure S3A of the Supporting Information). The  $\log(k_{on})$  values still show a V-shaped dependence but are clustered in a very narrow range for all three  $k_{on}$  parameters with values that are  $\sim 3$  orders of magnitude lower than those for the chelated model heme (Figure S3B of the Supporting Information, left). The  $\log(k_{off})$  plots show both  $k_{off}(\text{NO})$  and  $k_{off}(\text{O}_2)$  values that are greater than the  $k_{off}(\text{CO})$  values, a behavior that is different from that of heme proteins with a neutral proximal imidazole axial ligand and the P450-like proteins with a thiolate ligand. More work is needed to understand the structural and chemical bonding mechanisms that regulate binding of gas to the latter two classes of heme proteins.

## DISCUSSION

**Utility of the Sliding Scale Analysis for Understanding Ligand Discrimination.** Reduced pentacoordinate heme proteins with a neutral proximal histidine show innate chemical discrimination among NO, CO, and O<sub>2</sub>, just like the Fe(II)–imidazole heme model, even though the absolute affinities for any specific ligand can vary more than 1 million-fold (Figure 1). Extensive back bonding from the exogenous ligand to the iron d orbitals is allowed by the neutral axial imidazole and, coupled with the radical nature of NO, causes the  $K_D$  for NO binding to be roughly 10<sup>-3</sup>–10<sup>-4</sup>-fold smaller than that for CO binding, which in turn is 10<sup>-3</sup>–10<sup>-4</sup>-fold smaller than that for the binding of O<sub>2</sub>, which lacks the ability to back bond. Thus, plots of  $\log(K_D)$  versus ligand type for NO, CO, and O<sub>2</sub> are roughly linear and parallel for a wide variety of heme models and proteins that have apolar active sites and a neutral proximal histidine (Figures 1, 6, and 7). Studies of ligand binding parameters for synthetic model hemes designed to modulate the steric and electrostatic interaction seen in proteins are sporadic and incomplete<sup>14–16,68–72</sup> (Table S5 of the Supporting Information). We could not find another model heme compound, containing a proximal imidazole ligand, for which binding kinetic studies had been conducted with all three gases. Most experiments examined only O<sub>2</sub> and CO binding (e.g., ref 68) and were limited to compounds containing a proximal imidazole base.<sup>14–16,71,72</sup> However, the data that do exist show the general relationship  $K_D(\text{O}_2)/K_D(\text{CO}) \approx 10^3$ –10<sup>4</sup> for models with apolar distal regions, and this ratio is relatively insensitive to the degree of steric hindrance as indicated by a series of heme models with picket fence, strapped, pocket, and

capped distal pockets (Table S5 of the Supporting Information).<sup>68,71,73–75</sup> Only polar interactions or a severe steric effect that led to substantial porphyrin nonplanarity led to a marked lowering of this ratio.<sup>68,71,73–75</sup>

This linear relationship suggests a sliding scale along the  $y$ -axis of these plots and preservation of marked ligand discrimination, with the relative affinities always being in the following order: NO ≫ CO ≫ O<sub>2</sub>. The absolute affinity can be increased by facilitating or sterically pushing the proximal Fe–imidazole complex into the plane of the porphyrin ring to enhance the reactivity of the iron atom and/or by removing any steric constraints adjacent to the distal axial position. These structural effects in combination with the intrinsic chemical differences between the ligands lead to a remarkably wide range of ligand affinities, from 10<sup>-13</sup> to almost 1 M (Figures 1 and 7). This combination of ligand discrimination coupled with a much wider range of possible ligand binding affinities accounts for why gas sensor, storage, and transport heme proteins maintain the neutral form of the proximal imidazole.

In contrast, when the proximal ligand is a thiolate (P450-like heme proteins) or an imidazolate (peroxidases), there is very little equilibrium discrimination among NO, CO, and O<sub>2</sub>, and the range of absolute affinities is smaller, with  $K_D$  values ranging from 10<sup>-7</sup> to 10<sup>-3</sup> M. Thiolate is a very strong field ligand and highly electron-donating. As a result, there is strong competition for back bonding to the Fe(II) d<sub>2</sub> orbital with the distal gaseous ligand.<sup>31</sup> This competition with the thiolate exerts a leveling effect among NO, CO, and O<sub>2</sub> and, in general, decreases the Fe–XO bond strength and increases both the  $K_D$  and the  $k_{off}$  for all three gaseous ligands (Figure 8). Similar interpretations apply to peroxidases containing a proximal imidazolate ligand (Figure S3 of the Supporting Information). HRP, LPO, CcP, ascorbate peroxidase, lignin peroxidase, and peanut peroxidase all have a proximal histidine with imidazolate character due to H-bonding interactions with nearby proton bond acceptors (Asp or Asn).<sup>67</sup> These peroxidases all have negative midpoint potentials, and the strong electron donating or pushing effect by the imidazolate helps promote heterolytic cleavage of the O–O bond of bound peroxide, but at the expense of much weaker discrimination between the gaseous ligands and higher  $K_D$  values. Although crystallographic data for EPO are not available and MPO has an abnormally high midpoint potential and weak affinity for CO, biophysical studies have demonstrated that both peroxidases still have an imidazolate, proximal ligand,<sup>67</sup> accounting for their lack of discrimination between the gaseous ligands.

The sliding scale rule is also useful for predicting  $K_D$  values that are difficult or impossible to measure experimentally. Several NO-sensing heme proteins show very little or no reactivity toward O<sub>2</sub>, making it difficult to even estimate  $K_D(\text{O}_2)$ . However, it is straightforward to measure  $K_D(\text{CO})$  values for these proteins (Table 1 and Figure 1). If the sliding scale rule applies, the slopes of  $\log(K_D)$  versus ligand plots for model hemes or other proteins can be used to predict  $K_D(\text{O}_2)$  values for the NO sensors. This analysis is shown in Figure 1 for Ns H-NOX and sGC, and the predicted  $K_D$  values are ~0.005 and ~1 M, respectively. As shown in Figure 4, binding of O<sub>2</sub> to Ns H-NOX can be observed at high pressures, and the fitted value for  $K_D(\text{O}_2)$  was ~0.010 M, which on a logarithmic scale is very close to the predicted value and verifies the utility of the sliding scale rule. The value for sGC shows that it would require ≥100 atm of pure O<sub>2</sub> for the observation of any binding

713 at all (i.e.,  $\geq 10\%$  saturation), which accounts for why no  $O_2$   
714 binding has been observed and autoxidation occurs in days.

715 The sliding scale rule can also be used to predict  $K_D$ (NO)  
716 values of  $\sim 10^{-8}$  and  $\sim 10^{-10}$  M for sGC and Ns H-NOX,  
717 respectively, based on the measured  $K_D$ (CO) values for these  
718 NO sensors. Again, the predicted value for Ns H-NOX agrees  
719 well with that measured for the formation of the first 6c NO  
720 complex,<sup>13</sup> verifying our analysis. In contrast, the reported  $K_D$   
721 for binding of NO to sGC is  $\sim 1 \times 10^{-12}$  M, which is almost  
722 10000-fold smaller than the predicted value. However, the final  
723 sGC form is a 5c NO–heme complex with the proximal  
724 imidazole displaced. Thus, both the lack of correlation with the  
725 sliding scale rule and the change in proximal coordination  
726 geometry indicate a complex, multiple-step mechanism for  
727 binding of NO to sGC. Nonetheless, as shown in Figures 2 and  
728 3, the first NO binding step to form a transient 6c NO–heme–  
729 neutral imidazole complex shows a  $K_D$  of  $5 \times 10^{-8}$  M, which is  
730 remarkably close to the value predicted from the sliding scale  
731 rule and again verifies the utility of the sliding scale analysis.

732 **Oxygen Sensor, Storage, and Transport Heme  
733 Proteins.** Specific high-affinity  $O_2$  binding requires significant  
734 deviation from the sliding scale rule both to alter ligand  
735 discrimination and to decrease  $K_D(O_2)$  values into the  
736 micromolar range for sensing, transport, and storage and to  
737 the nanomolar range for  $O_2$  scavenging without oxidation. As  
738 described in previous work,<sup>32,76</sup> selective increases in  $O_2$  affinity  
739 are achieved by increased positive electrostatic fields adjacent to  
740 the Fe– $O_2$  complex and direct hydrogen bonding. As shown in  
741 Figures 1, 6, and 7, these favorable polar interactions can  
742 decrease the  $K_D(O_2)/K_D(CO)$  ratio from  $\sim 10000$  for apolar  
743 active sites to  $\leq 1.0$  in proteins where multiple hydrogen bonds  
744 are donated to bound  $O_2$ . The best example of a heme protein  
745 with a nanomolar  $K_D(O_2)$  and little or no CO binding is the  
746 domain 1 hemoglobin of *A. suum*, which is an obligate anaerobe  
747 in its adult stage and requires this globin to protect itself from  
748  $O_2$  poisoning (Figure 7 and ref 19). The sliding scale rule  
749 analyses in Figures 6 and 7 provide a concise way of quantifying  
750 and comparing the effects of distal pocket polarity on  
751 discrimination in favor of  $O_2$  binding.

752 **NO Sensors and Discrimination against NO Dioxyge-  
753 nation.** In the case of NO sensors, the problem is not  
754 equilibrium ligand discrimination. All proteins with a neutral  
755 proximal histidine and an apolar distal pocket have much higher  
756 affinities for NO than for either CO or  $O_2$ . Even in air ( $2.5 \times$   
757  $10^{-4}$  M  $O_2$ ) and low levels of NO ( $10^{-9}$  M), the  $K_D(O_2)/$   
758  $K_D(NO)$  ratio of  $10^8$  still favors reversible NO binding. The  
759 dilemma is NO dioxygenation by bound  $O_2$ , which destroys the  
760 signaling molecule. In air and low levels of NO,  $O_2$  will  
761 kinetically outcompete NO for initial binding to 5c Fe(II)-  
762 bound unliganded heme protein sensors because the values of  
763  $k_{on}(O_2)$  are normally only slightly smaller than those of  
764  $k_{on}(NO)$  (Figures 5–7). Then NO will react rapidly with the  
765 newly formed  $O_2$ –heme–imidazole complex to produce nitrate  
766 with a bimolecular rate constant roughly equal to that for  
767 simple binding of NO to the unliganded protein.<sup>77,78</sup> Thus, for  
768 a NO sensor to remain functional under aerobic conditions, it  
769 has to completely exclude  $O_2$  binding to prevent NO  
770 dioxygenation. This requirement has been achieved in Ns H-  
771 NOX, cyt c', and sGC by combinations of proximal restrictions  
772 and steric hindrance of the bound ligand, both of which  
773 markedly reduce ligand affinity. However, these structural  
774 effects also markedly increase the  $K_D$  for NO binding to form a  
775 conventional 6c NO–heme–imidazole complex (Scheme 1 for

776 sGC). On the basis of the sliding scale rule, the CO binding  
777 parameters for sGC predict a  $K_D(NO)$  value in the  $10^{-8}$  M  
778 region, which is too high for sensing nanomolar levels of the  
779 gas. Thus, sGC has evolved a complex multistep reaction  
780 mechanism in which the initial 6c NO complex converts to a  
781 high-affinity 5c complex by displacement of the proximal  
782 imidazole, a process that is accelerated by additional NO  
783 molecules (Scheme 1 and refs 27 and 79). The net result is a  
784 picomolar affinity of NO for sGC and total exclusion of  $O_2$   
785 binding even under aerobic conditions. Similar multistep NO  
786 reactions and  $O_2$  exclusion were also observed for cyt c', which  
787 shows high selectivity for NO. In this protein,  $O_2$  binding is  
788 excluded by distal steric hindrance from the L16 side chain<sup>26,27</sup>  
789 rather than the proximal strain as shown for sGC.  
790

791 The nitrophorin NO-storing protein found in insect salivary  
792 glands has adopted an alternative mechanism for preventing  $O_2$   
793 binding and dioxygenation. Nitrophorins exist in the Fe(III)  
794 state, which excludes  $O_2$  and CO binding, but can still bind  
795 NO, although with only micromolar  $K_D$  values. The high  $K_D$   
796 facilitates rapid displacement of NO by histamine after injection  
797 into mammalian hosts, which induces vasodilation and inhibits  
798 inflammation at the same time. This strategy of using Fe(III)  
799 binding is effective for NO storage and rapid release at high  
800 concentrations but not for sensing nanomolar levels of NO as a  
801 cell signaling molecule.  
802

## ■ CONCLUSIONS

802 Five-coordinate Fe(II) heme proteins with a neutral proximal  
803 His ligand strongly discriminate between the gaseous ligands,  
804 with affinities in the order  $NO \gg CO \gg O_2$  due to differential  
805 effects of back bonding and spin coupling. There is a linear  
806 dependence of  $\log(K_D)$  on ligand type for the NO, CO, and  $O_2$   
807 series, regardless of the absolute values for individual  
808 equilibrium dissociation constants. Deviations from this sliding  
809 scale rule do occur in heme proteins that function as relatively  
810 high-affinity  $O_2$  sensors, storage proteins, and transport  
811 proteins and have active site amino acids that can donate  
812 hydrogen bonds to the bound  $O_2$  molecule and preferentially  
813 lower  $K_D(O_2)$ . Cytochrome P450-like proteins and peroxidases  
814 contain strong field proximal thiolate and imidazolate ligands,  
815 which assist in heterolytic O–O bond cleavage of the substrate  
816 but compromise their ability to discriminate among NO, CO,  
817 and  $O_2$  binding. NO sensor proteins restrict the binding of all  
818 gaseous ligands by both proximal constraints of in-plane iron  
819 movement and direct hindrance of the bound ligand. These  
820 constraints effectively exclude  $O_2$  binding. High affinity for NO  
821 is achieved by a second step in which an ultrastable 5c NO–  
822 heme complex is formed by displacement of the distal His. This  
823 multistep mechanism appears to be a general strategy for all  
824 high-affinity NO sensors that need to exclude  $O_2$  binding to  
825 prevent dioxygenation of the signaling molecule.  
826

## ■ ASSOCIATED CONTENT

### S Supporting Information

827 Binding parameter values for NO, CO, and  $O_2$  of Mb single  
828 mutants (Table S1), other globins (Table S2), heme proteins  
829 containing a thiolate proximal ligand (Table S3), heme proteins  
830 containing a proximal imidazolate ligand (Table S4), and a  
831 panel of picket fence, pocketed, strapped, and capped heme  
832 models (Table S5) and correlational plots between binding  
833 parameters and ligand types for the Mb double mutants (Figure  
834 S1), triple mutants (Figure S2), and peroxidases with  
835

836 imidazolate proximal ligands (Figure S3). This material is  
837 available free of charge via the Internet at <http://pubs.acs.org>.

## 838 ■ AUTHOR INFORMATION

### 839 Corresponding Author

840 \*Division of Hematology, Internal Medicine, University of  
841 Texas Medical School at Houston, MSB 5290, 6431 Fannin,  
842 Houston, TX 77030. Phone: (713) 500-6771. Fax: (713) 500-  
843 6810. E-mail: Ah-lim.tsai@uth.tmc.edu.

### 844 Funding

845 This work was supported by National Heart, Lung, and Blood  
846 Institute Grants HL095820 (A.-L.T.), HL088128 (E.M.), and  
847 HL047020 (J.S.O.), National Institute of General Medical  
848 Sciences Grant GM035649 (J.S.O.), the American Heart  
849 Association, South Central Affiliate, Grant-in-Aid  
850 09GRNT2060182 (E.M.), and The Robert A. Welch  
851 Foundation Grant C-0612 (J.S.O.).

## 852 ■ ACKNOWLEDGMENTS

853 We thank Dr. Lee-Ho Wang for providing us with a  
854 prostacyclin synthase sample for NO binding kinetic measure-  
855 ments and Dr. Wen Liu for establishing the expression system  
856 for Ns H-NOX and purifying the recombinant protein for our  
857 oxygen binding experiment. We also thank Professor Joseph  
858 Bonaventura for suggesting that we try high-pressure cell  
859 binding of O<sub>2</sub> to the sensors at the Gordon Research  
860 Conference on Nitric Oxide, 2011. Finally, we acknowledge  
861 the strong influence that Vijay S. Sharma and Teddy G. Traylor  
862 had on our thinking about ligand discrimination and binding of  
863 NO to heme proteins. Their ideas published and shared with  
864 one of us (J.S.O.) in the late 1980s were among the first to  
865 recognize the importance of distal pocket polarity in  
866 preferentially stabilizing bound O<sub>2</sub> in globins and formation  
867 of pentacoordinate NO–heme complexes in NO sensors.

## 868 ■ ABBREVIATIONS

869 NO, nitric oxide; CO, carbon monoxide; O<sub>2</sub>, dioxygen; DTT,  
870 dithiothreitol; β-BME, mercaptoethanol; IPTG, isopropyl 1-  
871 thio-β-D-galactopyranoside; cGMP, cyclic GMP; Mb, myoglo-  
872 bin; Fe(II), ferrous heme; Fe(III), ferric heme; 5c, five-  
873 coordinate; 6c, six-coordinate; 5c-NO, five-coordinate NO–  
874 heme complex; 6c-NO, six-coordinate NO–heme complex;  
875 Hb, hemoglobin; H-NOX, heme-nitric oxide and oxygen  
876 binding; Ns H-NOX, *Nostoc* sp. H-NOX; Tt H-NOX,  
877 *Thermoanaerobacter tengcongensis* H-NOX; sGC, soluble  
878 guanylyl cyclase; αβI145Y sGC, sGC containing the I145Y  
879 mutation in the β subunit; cyt c', cytochrome c'; CB, *Clostridium*  
880 *botulinum*; Lb, plant hemoglobins, leghemoglobin; rHb, rice  
881 hemoglobin; Asc Hb, invertebrate Hb from *A. suum*; FHb,  
882 flavohemoglobins; trHbs, truncated Hbs; trHbN and trHbO,  
883 trHbs from *M. tuberculosis*; trCb, single-domain trHb from *C.*  
884 *jejuni*; Ngb, neuroglobin; CLP, chloroperoxidase; PGIS,  
885 prostacyclin synthase; HRP, horseradish peroxidase; LPO,  
886 lactoperoxidase; EPO, eosinophil peroxidase; CcP, cytochrome  
887 c peroxidase; MPO, myeloperoxidase; EPR, electron para-  
888 magnetic resonance spectroscopy.

## 889 ■ REFERENCES

890 (1) Messerschmidt, A., Huber, R., Poulos, T., and Wieghardt, K., Eds.  
891 (2001) *Handbooks of metalloproteins*, Vol. 1, John Wiley and Sons, Ltd.,  
892 Chichester, U.K.

- (2) Turano, P., and Lu, Y. (2001) Iron in heme and related proteins. In *Handbook on Metalloproteins* (Bertini, I., Sigel, A., and Sigel, H., Eds.) pp 269–342, Marcel Dekker, Inc., New York. 894
- (3) Olson, J. S., and Phillips, G. N. J. (1997) Myoglobin discriminates between O<sub>2</sub>, NO, and CO by electrostatic interactions with the bound ligand. *J. Biol. Inorg. Chem.* 2, 544–552. 898
- (4) Walker, F. A. (2005) Nitric oxide interaction with insect nitrophorins and thoughts on the electron configuration of the [FeNO]<sub>6</sub> complex. *J. Inorg. Biochem.* 99, 216–236. 901
- (5) Dunham, C. M., Dioum, E. M., Tuckerman, J. R., Gonzalez, G., Scott, W. G., and Gilles-Gonzalez, M. A. (2003) A distal arginine in oxygen-sensing heme-PAS domains is essential to ligand binding, signal transduction, and structure. *Biochemistry* 42, 7701–7708. 905
- (6) Aono, S. (2003) Biochemical and biophysical properties of the CO-sensing transcriptional activator CooA. *Acc. Chem. Res.* 36, 825–831. 907
- (7) Derbyshire, E. R., and Marletta, M. A. (2009) Biochemistry of soluble guanylate cyclase. *Handb. Exp. Pharmacol.*, 17–31. 910
- (8) Zhao, Y., Brandish, P. E., Ballou, D. P., and Marletta, M. A. (1999) A molecular basis for nitric oxide sensing by soluble guanylate cyclase. *Proc. Natl. Acad. Sci. U.S.A.* 96, 14753–14758. 913
- (9) Martin, E., Berka, V., Bogatenkova, E., Murad, F., and Tsai, A. L. (2006) Ligand selectivity of soluble guanylyl cyclase: Effect of the hydrogen bonding tyrosine in the distal heme pocket on binding of oxygen, nitric oxide and carbon monoxide. *J. Biol. Chem.* 281, 27836–27845. 914
- (10) Yeh, H. C., Hsu, P. Y., Wang, J. S., Tsai, A. L., and Wang, L. H. (2005) Characterization of heme environment and mechanism of peroxide bond cleavage in human prostacyclin synthase. *Biochim. Biophys. Acta* 1738, 121–132. 919
- (11) Yeh, H. C., Tsai, A. L., and Wang, L. H. (2007) Reaction mechanisms of 15-hydroperoxyeicosatetraenoic acid catalyzed by human prostacyclin and thromboxane synthases. *Arch. Biochem. Biophys.* 461, 159–168. 924
- (12) Scott, E. E., and Gibson, Q. H. (1997) Ligand migration in sperm whale myoglobin. *Biochemistry* 36, 11909–11917. 928
- (13) Tsai, A. L., Berka, V., Martin, F. E., Ma, X., van den Akker, F., Fabian, M., and Olson, J. S. (2010) Is *Nostoc* H-NOX an NO sensor or Redox Switch? *Biochemistry* 49, 6587–6599. 931
- (14) Rose, E. J., Venkatasubramanian, P. N., Swartz, J. C., Jones, R. D., Basolo, F., and Hoffman, B. M. (1982) Carbon monoxide binding kinetics in “capped” porphyrin compounds. *Proc. Natl. Acad. Sci. U.S.A.* 79, 5742–5745. 932
- (15) Chang, C. K., and Traylor, T. G. (1975) Reversible oxygenation of protoheme-imidazole complex in aqueous solution. *Biochem. Biophys. Res. Commun.* 62, 729–735. 936
- (16) Hoshino, M., Ozawa, K., Seki, H., and Ford, P. C. (1993) Photochemistry of nitric oxide adducts of water-soluble iron(III) porphyrin and ferrihemoproteins studied by nanosecond laser photolysis. *J. Am. Chem. Soc.* 115, 9568–9575. 939
- (17) Carver, T. E., Brantley, R. E. Jr., Singleton, E. W., Arduini, R. M., Quillin, M. L., Phillips, G. N. Jr., and Olson, J. S. (1992) A novel site-directed mutant of myoglobin with an unusually high O<sub>2</sub> affinity and low autoxidation rate. *J. Biol. Chem.* 267, 14443–14450. 944
- (18) Quillin, M. L., Li, T., Olson, J. S., Phillips, G. N. Jr., Dou, Y., Ikeda-Saito, M., Regan, R., Carlson, M., Gibson, Q. H., Li, H., et al. (1995) Structural and functional effects of apolar mutations of the distal valine in myoglobin. *J. Mol. Biol.* 245, 416–436. 948
- (19) Draghi, F., Miele, A. E., Travaglini-Allicatelli, C., Vallone, B., Brunori, M., Gibson, Q. H., and Olson, J. S. (2002) Controlling ligand binding in myoglobin by mutagenesis. *J. Biol. Chem.* 277, 7509–7519. 952
- (20) Stone, J. R., and Marletta, M. A. (1995) The ferrous heme of soluble guanylyl cyclase: Formation of hexacoordinate complexes with carbon monoxide and nitrosomethane. *Biochemistry* 34, 16397–16403. 954
- (21) Boon, E. M., Huang, S. H., and Marletta, M. A. (2005) A molecular basis for NO selectivity in soluble guanylyl cyclase. *Nat. Chem. Biol.* 1, 53–59. 958

- 961 (22) Stone, J. R., and Marletta, M. A. (1996) Spectral and kinetic  
962 studies on the activation of soluble guanylate cyclase by nitric oxide.  
963 *Biochemistry* 35, 1093–1099.
- 964 (23) Kassner, R. J. (1991) Ligand binding properties of cytochromes  
965 c'. *Biochim. Biophys. Acta* 1058, 8–12.
- 966 (24) George, S. J., Andrew, C. R., Lawson, D. M., Thorneley, R. N.,  
967 and Eady, R. R. (2001) Stopped-flow infrared spectroscopy reveals a  
968 six-coordinate intermediate in the formation of the proximally bound  
969 five-coordinate NO adduct of cytochrome c'. *J. Am. Chem. Soc.* 123,  
970 9683–9684.
- 971 (25) Andrew, C. R., George, S. J., Lawson, D. M., and Eady, R. R.  
972 (2002) Six- to five-coordinate heme-nitrosyl conversion in cytochrome  
973 c' and its relevance to guanylate cyclase. *Biochemistry* 41, 2353–2360.
- 974 (26) Antonyuk, S. V., Rustage, N., Petersen, C. A., Arnst, J. L., Heyes,  
975 D. J., Sharma, R., Berry, N. G., Scrutton, N. S., Eady, R. R., Andrew, C.  
976 R., and Hasnain, S. S. (2011) Carbon monoxide poisoning is  
977 prevented by the energy costs of conformational changes in gas-  
978 binding haemproteins. *Proc. Natl. Acad. Sci. U.S.A.* 108, 15780–15785.
- 979 (27) Hough, M. A., Antonyuk, S. V., Barbieri, S., Rustage, N., McKay,  
980 A. L., Servid, A. E., Eady, R. R., Andrew, C. R., and Hasnain, S. S.  
981 (2011) Distal-to-proximal NO conversion in hemoproteins: The role  
982 of the proximal pocket. *J. Mol. Biol.* 405, 395–409.
- 983 (28) Zhang, W., Olson, J. S., and Phillips, G. N. Jr. (2005)  
984 Biophysical and kinetic characterization of HemAT, an aerotaxis  
985 receptor from *Bacillus subtilis*. *Biophys. J.* 88, 2801–2814.
- 986 (29) Tsai, A.-L. (1994) How does NO activate hemoproteins? *FEBS*  
987 *Lett.* 341, 141–145.
- 988 (30) Spiro, T. G., and Jarzecki, A. A. (2001) Heme-based sensors:  
989 Theoretical modeling of heme-ligand-protein interactions. *Curr. Opin.*  
990 *Chem. Biol.* 5, 715–723.
- 991 (31) Spiro, T. G., Zgierski, M. Z., and Kozlowski, P. M. (2001)  
992 Stereoelectronic factors in CO, NO and O<sub>2</sub> binding to heme from  
993 vibrational spectroscopy and DFT analysis. *Coord. Chem. Rev.* 219–  
994 221, 923–936.
- 995 (32) Phillips, G. N. Jr., Teodoro, M. L., Li, T., Smith, B., and Olson, J.  
996 S. (1999) Bound CO is a molecular probe of electrostatic potential in  
997 the distal pocket of myoglobin. *J. Phys. Chem. B* 103, 8817–8829.
- 998 (33) Coyle, C. M., Vogel, K. M., Rush, T. S. III, Kozlowski, P. M.,  
999 Williams, R., Spiro, T. G., Dou, Y., Ikeda-Saito, M., Olson, J. S., and  
1000 Zgierski, M. Z. (2003) FeNO structure in distal pocket mutants of  
1001 myoglobin based on resonance Raman spectroscopy. *Biochemistry* 42,  
1002 4896–4903.
- 1003 (34) Kharitonov, V. G., Russwurm, M., Magde, D., Sharma, V. S., and  
1004 Koesling, D. (1997) Dissociation of nitric oxide from soluble guanylate  
1005 cyclase. *Biochem. Biophys. Res. Commun.* 239, 284–286.
- 1006 (35) Sharma, V. S., Traylor, T. G., Gardiner, R., and Mizukami, H.  
1007 (1987) Reaction of nitric oxide with heme proteins and model  
1008 compounds of hemoglobin. *Biochemistry* 26, 3837–3843.
- 1009 (36) Kharitonov, V. G., Sharma, V. S., Magde, D., and Koesling, D.  
1010 (1997) Kinetics of nitric oxide dissociation from five- and six-  
1011 coordinate nitrosyl hemes and heme proteins, including soluble  
1012 guanylate cyclase. *Biochemistry* 36, 6814–6818.
- 1013 (37) Franzen, S. (2002) Spin-dependent mechanism for diatomic  
1014 ligand binding to heme. *Proc. Natl. Acad. Sci. U.S.A.* 99, 16754–16759.
- 1015 (38) Strickland, N., and Harvey, J. N. (2007) Spin-forbidden ligand  
1016 binding to the ferrous-heme group: Ab initio and DFT studies. *J. Phys.*  
1017 *Chem. B* 111, 841–852.
- 1018 (39) Harvey, J. N. (2000) DFT computation of the intrinsic barrier  
1019 to CO geminate recombination with heme compounds. *J. Am. Chem.*  
1020 *Soc.* 122, 12401–12402.
- 1021 (40) Ionascu, D., Gruia, F., Ye, X., Yu, A., Rosca, F., Beck, C.,  
1022 Demidov, A., Olson, J. S., and Champion, P. M. (2005) Temperature-  
1023 dependent studies of NO recombination to heme and heme proteins.  
1024 *J. Am. Chem. Soc.* 127, 16921–16934.
- 1025 (41) Olson, J. S., and Phillips, G. N. Jr. (1996) Kinetic Pathways and  
1026 Barriers for Ligand Binding to Myoglobin. *J. Biol. Chem.* 271, 17596.
- 1027 (42) Dou, Y., Maillett, D. H., Eich, R. F., and Olson, J. S. (2002)  
1028 Myoglobin as a model system for designing heme protein based blood  
1029 substitutes. *Biophys. Chem.* 98, 127–148.
- 1030 (43) Eich, R. F. (1997) Reactions of Nitric Oxide with Myoglobin. In *Biochemistry and Cell Biology*, Rice University, Houston. 1031
- 1031 (44) Foley, E. W. (2005) Physiologically Relevant Reactions of 1032 Myoglobin and Hemoglobin with NO. In *Biochemistry and Cell Biology*, 1033 Rice University, Houston. 1034
- 1035 (45) Coyle, C. M., Puranik, M., Youn, H., Nielsen, S. B., Williams, R.  
1036 D., Kerby, R. L., Roberts, G. P., and Spiro, T. G. (2003) Activation 1036 mechanism of the CO sensor CooA. Mutational and resonance Raman 1037 spectroscopic studies. *J. Biol. Chem.* 278, 35384–35393. 1038
- 1039 (46) Hargrove, M. S., Barry, J. K., Brucker, E. A., Berry, M. B.,  
1040 Phillips, G. N. Jr., Olson, J. S., Arredondo-Peter, R., Dean, J. M.,  
1041 Klucas, R. V., and Sarath, G. (1997) Characterization of recombinant 1041 soybean leghemoglobin a and apolar distal histidine mutants. *J. Mol.* 1042 *Biol.* 266, 1032–1042. 1043
- 1044 (47) Arredondo-Peter, R., Hargrove, M. S., Sarath, G., Moran, J. F.,  
1045 Lohrman, J., Olson, J. S., and Klucas, R. V. (1997) Rice hemoglobins. 1045 Gene cloning, analysis, and O<sub>2</sub>-binding kinetics of a recombinant 1046 protein synthesized in *Escherichia coli*. *Plant Physiol.* 115, 1259–1266. 1047
- 1048 (48) Lu, C., Egawa, T., Mukai, M., Poole, R. K., and Yeh, S. R. (2008) 1049 Hemoglobins from *Mycobacterium tuberculosis* and *Campylobacter* 1049 *jejuni*: A comparative study with resonance Raman spectroscopy. 1050 *Methods Enzymol.* 437, 255–286. 1051
- 1052 (49) Van Doorslaer, S., Dewilde, S., Kiger, L., Nistor, S. V.,  
1053 Goovaerts, E., Marden, M. C., and Moens, L. (2003) Nitric oxide 1053 binding properties of neuroglobin. A characterization by EPR and flash 1054 photolysis. *J. Biol. Chem.* 278, 4919–4925. 1055
- 1056 (50) Abu-Soud, H. M., Gachhui, R., Raushel, F. M., and Stuehr, D. J. 1056 (1997) The ferrous-dioxy complex of neuronal nitric oxide synthase. 1057 Divergent effects of L-arginine and tetrahydrobiopterin on its stability. 1058 *J. Biol. Chem.* 272, 17349–17353. 1059
- 1060 (51) Abu-Soud, H. M., Wu, C., Ghosh, D. K., and Stuehr, D. J. 1060 (1998) Stopped-flow analysis of CO and NO binding to inducible 1061 nitric oxide synthase. *Biochemistry* 37, 3777–3786. 1062
- 1063 (52) Franke, A., Stochel, G., Jung, C., and Van Eldik, R. (2004) 1063 Substrate binding favors enhanced NO binding to P450cam. *J. Am.* 1064 *Chem. Soc.* 126, 4181–4191. 1065
- 1066 (53) Gerber, N. C., and Sligar, S. G. (1992) Catalytic mechanism of 1066 cytochrome P-450: Evidence for a distal charge relay. *J. Am. Chem. Soc.* 1067 114, 8742–8743. 1068
- 1069 (54) Sevrioukova, I. F., and Peterson, J. A. (1995) Reaction of carbon 1069 monoxide and molecular oxygen with P450terp (CYP108) and 1070 P450BM-3 (CYP102). *Arch. Biochem. Biophys.* 317, 397–404. 1071
- 1072 (55) Quaroni, L. G., Seward, H. E., McLean, K. J., Girvan, H. M., Ost, 1072 T. W., Noble, M. A., Kelly, S. M., Price, N. C., Cheesman, M. R., 1073 Smith, W. E., and Munro, A. W. (2004) Interaction of nitric oxide with 1074 cytochrome P450 BM3. *Biochemistry* 43, 16416–16431. 1075
- 1076 (56) Lambeir, A. M., and Dunford, H. B. (1985) Oxygen binding to 1076 dithionite-reduced chloroperoxidase. *Eur. J. Biochem.* 147, 93–96. 1077
- 1078 (57) Lange, R., Heiber-Langer, I., Bonfils, C., Fabre, I., Negishi, M., 1078 and Balny, C. (1994) Activation volume and energetic properties of 1079 the binding of CO to hemoproteins. *Biophys. J.* 66, 89–98. 1080
- 1081 (58) Yeh, H. C., Hsu, P. Y., Tsai, A. L., and Wang, L. H. (2008) 1081 Spectroscopic characterization of the oxyferrous complex of 1082 prostacyclin synthase in solution and in trapped sol-gel matrix. *FEBS* 1083 *J.* 275, 2305–2314. 1084
- 1085 (59) Yeh, H. C., Hsu, P. Y., Wang, J. S., Tsai, A. L., and Wang, L. H. 1085 (2005) Characterization of heme environment and mechanism of 1086 peroxide bond cleavage in human prostacyclin synthase. *Biochim.* 1087 *Biophys. Acta* 1738, 121–132. 1088
- 1089 (60) Coletta, M., Ascoli, F., Brunori, M., and Traylor, T. G. (1986) 1089 pH dependence of carbon monoxide binding to ferrous horseradish 1090 peroxidase. *J. Biol. Chem.* 261, 9811–9814. 1091
- 1092 (61) Rodriguez-Lopez, J. N., Smith, A. T., and Thorneley, R. N. 1092 (1997) Effect of distal cavity mutations on the binding and activation 1093 of oxygen by ferrous horseradish peroxidase. *J. Biol. Chem.* 272, 389– 1094 395. 1095
- 1096 (62) Abu-Soud, H. M., and Hazen, S. L. (2001) Interrogation of 1096 heme pocket environment of mammalian peroxidases with diatomic 1097 ligands. *Biochemistry* 40, 10747–10755. 1098

- 1099 (63) Galijasevic, S., Saed, G. M., Diamond, M. P., and Abu-Soud, H.  
1100 M. (2004) High dissociation rate constant of ferrous-dioxy complex  
1101 linked to the catalase-like activity in lactoperoxidase. *J. Biol. Chem.* 279,  
1102 39465–39470.
- 1103 (64) Babcock, G. T., and Wikstrom, M. (1992) Oxygen activation  
1104 and the conservation of energy in cell respiration. *Nature* 356, 301–  
1105 309.
- 1106 (65) Mims, M. P., Porras, A. G., Olson, J. S., Noble, R. W., and  
1107 Peterson, J. A. (1983) Ligand binding to heme proteins. An evaluation  
1108 of distal effects. *J. Biol. Chem.* 258, 14219–14232.
- 1109 (66) Jantschko, W., Furtmuller, P. G., Zederbauer, M., Jakopitsch, C.,  
1110 and Obinger, C. (2004) Kinetics of oxygen binding to ferrous  
1111 myeloperoxidase. *Arch. Biochem. Biophys.* 426, 91–97.
- 1112 (67) Murphy, E. J., Marechal, A., Segal, A. W., and Rich, P. R. (2010)  
1113 CO binding and ligand discrimination in human myeloperoxidase.  
1114 *Biochemistry* 49, 2150–2158.
- 1115 (68) Collman, J. P., Boulatov, R., Sunderland, C. J., and Fu, L. (2004)  
1116 Functional analogues of cytochrome c oxidase, myoglobin, and  
1117 hemoglobin. *Chem. Rev.* 104, 561–588.
- 1118 (69) Collman, J. P., and Reed, C. A. (1973) Syntheses of ferrous-  
1119 porphyrin complexes. A hypothetical model for deoxymyoglobin. *J.*  
1120 *Am. Chem. Soc.* 95, 2048–2049.
- 1121 (70) Ford, P. C., and Lorkovic, I. M. (2002) Mechanistic aspects of  
1122 the reactions of nitric oxide with transition-metal complexes. *Chem.*  
1123 *Rev.* 102, 993–1018.
- 1124 (71) Tani, F., Matsu-ura, M., Ariyama, K., Setoyama, T., Shimada, T.,  
1125 Kobayashi, S., Hayashi, T., Matsuo, T., Hisaeda, Y., and Naruta, Y.  
1126 (2003) Iron twin-coronet porphyrins as models of myoglobin and  
1127 hemoglobin: Amphibious electrostatic effects of overhanging hydroxyl  
1128 groups for successful CO/O<sub>2</sub> discrimination. *Chemistry* 9, 862–870.
- 1129 (72) Chang, C. K., and Traylor, T. G. (1975) Kinetics of oxygen and  
1130 carbon monoxide binding to synthetic analogs of the myoglobin and  
1131 hemoglobin active sites. *Proc. Natl. Acad. Sci. U.S.A.* 72, 1166–1170.
- 1132 (73) Collman, J. P., Brauman, J. I., Iverson, B. L., Sessler, J. L., Morris,  
1133 R. M., and Gibson, Q. H. (1983) O<sub>2</sub> and CO binding to iron(II)  
1134 porphyrins: A comparison of the “picket fence” and “pocket”  
1135 porphyrins. *J. Am. Chem. Soc.* 105, 3052–3064.
- 1136 (74) Shantha, D., James, B. R., Dolphin, D., Traylor, T. G., and  
1137 Lopez, M. A. (1994) Dioxygen and carbon monoxide binding to apolar  
1138 cyclophane hemes: Durene-capped hemes. *J. Am. Chem. Soc.* 116, 6–  
1139 14.
- 1140 (75) Tetreau, C., Lavalette, D., Momenteau, M., Fischer, J., and  
1141 Weiss, R. (1994) Structure-reactivity relationship in oxygen and  
1142 carbon monoxide binding with some heme models. *J. Am. Chem. Soc.*  
1143 116, 11840–11848.
- 1144 (76) Smagghe, B. J., Halder, P., and Hargrove, M. S. (2008)  
1145 Measurement of distal histidine coordination equilibrium and kinetics  
1146 in hexacoordinate hemoglobins. *Methods Enzymol.* 436, 359–378.
- 1147 (77) Eich, R. F., Li, T., Lemon, D. D., Doherty, D. H., Curry, S. R.,  
1148 Aitken, J. F., Mathews, A. J., Johnson, K. A., Smith, R. D., Phillips, G.  
1149 N. Jr., and Olson, J. S. (1996) Mechanism of NO-induced oxidation of  
1150 myoglobin and hemoglobin. *Biochemistry* 35, 6976–6983.
- 1151 (78) Gardner, P. R., Gardner, A. M., Brashear, W. T., Suzuki, T.,  
1152 Hvítved, A. N., Setchell, K. D., and Olson, J. S. (2006) Hemoglobins  
1153 dioxygenate nitric oxide with high fidelity. *J. Inorg. Biochem.* 100, 542–  
1154 550.
- 1155 (79) Tsai, A. L., Berka, V., Sharina, I., and Martin, E. (2011) Dynamic  
1156 ligand exchange in soluble guanylyl cyclase: Implications for sGC  
1157 regulation and desensitization. *J. Biol. Chem.*



in press